

Charmless hadronic decays $B \rightarrow PP, PV, VV$ and new physics effects in the general two-Higgs doublet models

Zhenjun Xiao^(1,2) *, Chong Sheng Li⁽¹⁾

1. Department of Physics, Peking University, Beijing, 100871, People's Republic of China
2. Department of Physics, Henan Normal University, Xinxiang, Henan, 453002, People's Republic of China

Kuang-Ta Chao

CCAST(World Laboratory), P.O.Box 8730, Beijing 100080, People's Republic of China
and Department of Physics, Peking University, Beijing, 100871, People's Republic of China
(December 2, 2024)

Abstract

Based on the low-energy effective Hamiltonian with generalized factorization, we calculate the new physics contributions to the branching ratios of the two-body charmless hadronic decays of B_u and B_d mesons induced by the new gluonic and electroweak charged-Higgs penguin diagrams in the general two-Higgs doublet models (models I, II and III). Within the considered parameter space, we find that: (a) the new physics effects from new gluonic penguin diagrams strongly dominate over those from the new γ - and Z^0 - penguin diagrams; (b) in models I and II, new physics contributions to most studied B meson decay channels are rather small in size: from -15% to 20% ; (c) in model III, however, the new physics enhancements to penguin-dominated decay modes can be significant, $\sim (30-200)\%$, and therefore are measurable in forthcoming high precision B experiments; (d) the new physics enhancements to ratios $\mathcal{B}(B \rightarrow K\eta')$ are significant in model III, $\sim (35-70)\%$, and hence provide a simple and plausible new physics interpretation for the observed unexpectedly large $B \rightarrow K\eta'$ decay rates; (e) the theoretical predictions for $\mathcal{B}(B \rightarrow K^+\pi)$ and $\mathcal{B}(B \rightarrow K^0\pi^+)$ in model III are still consistent with the data within 2σ errors; (f) the significant new physics enhancements to the branching ratios of $B \rightarrow K^0\pi^0, K^{*0}\eta, K^{*+}\pi^-, K^+\phi, K^{*0}\omega, K^{*+}\phi$ and $K^{*0}\phi$ decays are helpful to improve the agreement between the data and theoretical predictions; (g) the theoretical predictions of $\mathcal{B}(B \rightarrow PP, PV, VV)$ in the 2HDM's are generally consistent with experimental measurements and upper limits ($90\%C.L.$)

PACS numbers: 13.25.Hw, 12.15.Ji, 12.38.Bx, 12.60.Fr

*E-mail: zxiao@ibm320h.phy.pku.edu.cn

I. INTRODUCTION

The main objective of B experiments is to explore in detail the physics of CP violation, to determine many of the flavor parameters of the standard model (SM) at high precision, and to probe for possible effects of new physics beyond the SM [1–3]. Precision measurements of B meson system can provide an insight into very high energy scales via the indirect loop effects of new physics. The B system therefore offers a complementary probe to the search for new physics at the Tevatron, LHC and NLC [1].

In B experiments, new physics beyond the SM may manifest itself, for example, in following two ways [1,3]: (a) decays which are expected to be rare in the SM are found to have large branching ratios; (b) CP-violating asymmetries which are expected to vanish or be very small in the SM are found to be significantly large or with a very different pattern with what predicted in the SM. These potential deviations may be induced by the virtual effects of new physics through loop diagrams.

It is well known that the two-body charmless hadronic decays $B \rightarrow h_1 h_2$ (where h_1 and h_2 are the light pseudo-scalar (P) and/or vector(V) mesons) play a very important role in studying CP violation and the heavy flavor physics [4,5]. Several groups [6–9] recently presented their systematic calculations for these B decay channels in the SM by using the low energy effective Hamiltonian [10–12] with the generalized factorization approach [7,13–15].

Theoretically, the effective Hamiltonian is our basic tool to calculate the branching ratios and A_{CP} of B meson decays. The short and long distance QCD effects in the hadronic decays are separated by means of the operator product expansion [16]. The short-distance QCD corrected Lagrangian at next-to-leading order (NLO) is available now, but we still do not know how to calculate hadronic matrix element from first principles. One conventionally resort to the factorization ansatz [13]. However, we also know that non-factorizable contribution really exists and can not be neglected numerically for most hadronic B decay channels. To remedy factorization hypothesis, some authors [7,14,15] introduced a phenomenological parameter N^{eff} (i.e. the effective number of color) to model the non-factorizable contribution to hadronic matrix element, which is commonly called generalized factorization. On the other hand, as pointed by Buras and Silverstrini [17], such generalization suffers from the problems of gauge and infrared dependence since the constant matrix \hat{r}_V appeared in the expressions of C_i^{eff} depends on both the gauge chosen and the external momenta. Very recently, Cheng *et al.* [18] studied and resolved above controversies on the gauge dependence and infrared singularity of C_i^{eff} by using the perturbative QCD factorization theorem. Besides the generalized factorization approach, a new approach, called as the QCD factorization [19], appeared recently [19,20], in which the decay amplitude is described by a kernel containing the ‘hard’ interaction given by a perturbatively evaluated effective Hamiltonian folded with form factors, decay constants and light-cone distributions of mesons into which the long distance effects are lumped. And some two-body hadronic B meson decays, such as $B \rightarrow \pi\pi$ and $K\pi$ modes, have been calculated in this approach [19–21].

On the experimental side, CLEO collaboration reported the observations of thirteen $B \rightarrow PP, PV$ decay channels and set new upper limits for many other decay modes [22–25]. The BaBar and Belle collaboration at SLAC and KEK also presented their first observation for some $B \rightarrow PP, PV$ decays at the ICHEP 2000 conference [26,27]. Except for the decay channels $B \rightarrow K\eta'$, the measured branching ratios for $B \rightarrow h_1 h_2$ decays are generally in

good agreement with the SM theoretical predictions based on effective Hamiltonian with factorization. Unexpectedly large $B \rightarrow K\eta'$ rates was firstly reported by CLEO in 1997 [28], and confirmed very recently by CLEO and BaBar Collaborations [23,29,26]. Although many possible mechanisms such as gluon and/or charm content in η' and the hairpin diagram have been considered in order to increase the theoretical predictions of $\mathcal{B}(B \rightarrow \eta')$, it is now still difficult to explain the observed large rate for $B \rightarrow K\eta'$ decays [23,26,29]. This fact strongly suggest the requirement for additional contributions unique to the η' meson in the framework of the SM, or large enhancements from new physics beyond the SM.

According to the studies in Refs. [30–33], we know that (a) an enhanced $b \rightarrow sg$ can lead to a large $\mathcal{B}(B \rightarrow \eta' X_s)$, (b) the possible contributions to the ratio $b \rightarrow sg$ in both type I and II two-Higgs-doublet models (2HDM) are not large enough to meet the requirement [30,31]. Very recently, we calculated [34,35] the new physics enhancements to the branching ratios $\mathcal{B}(b \rightarrow sg)$ and $\mathcal{B}(b \rightarrow q'q\bar{q})$ with $q' \in \{d, s\}$ and $q \in \{u, d, s\}$ induced by charged-Higgs gluonic penguin diagrams in model III (the third type of 2HDM) with inclusion of NLO QCD corrections [36], and found that the rate of $b \rightarrow sg$ in model III can be enhanced significantly. The predicted charm multiplicity n_c consequently become consistent with the measured n_c , while the agreement between the theoretical prediction and the data of \mathcal{B}_{SL} is also improved by inclusion of new physics effects.

In this paper we will calculate the new physics contributions to the branching ratios of exclusive two-body charmless hadronic decays $B \rightarrow PP, PV, VV$ ¹ from new gluonic and electroweak charged-Higgs penguin diagrams in the general two-Higgs-doublet models. We try to check the size and pattern of new physics effects on the exclusive two-body charmless B meson decays and to see if the new physics contributions in the model III can be large enough to provide the required enhancement for $B \rightarrow K\eta'$ decay modes. We will present our systematic calculation of branching ratios for seventy six $B \rightarrow h_1 h_2$ decay modes by employing the effective Hamiltonian with generalized factorization [7,9]. We will evaluate analytically all new strong and electroweak penguin diagrams induced by exchanges of charged Higgs bosons in the quark level processes $b \rightarrow qV^*$ with $q \in \{d, s\}$ and $V \in \{gluon, \gamma, Z\}$, and then combine the new physics contributions with their SM counterparts and finally calculate the branching ratios for all seventy six exclusive $B \rightarrow h_1 h_2$ decay modes.

This paper is organized as follows. In Sec.II, we describe the basic structures of the 2HDM's and examine the allowed parameter space of the general 2HDM's from currently available data. In Sec. III, we evaluate analytically the new penguin diagrams, combine the new physics contributions with their SM counterparts and find the effective Wilson coefficients C_i^{eff} . In Sec. IV, we present the formulae needed to calculate the branching ratios $\mathcal{B}(B \rightarrow h_1 h_2)$. In the following three sections, we calculate and show numerical results of branching ratios for $B \rightarrow PP, PV$ and VV decay modes, respectively. We concentrate on those decay modes with well-measured branching ratios and sizable yields. The conclusions and discussions are included in the final section.

¹In the following, B always means B_u or B_d mesons. We here do not consider the decays of B_s meson.

II. THE GENERAL 2HDM AND EXPERIMENTAL CONSTRAINTS

The simplest extension of the SM is the so-called two-Higgs-doublet models [37]. In such models, the tree level flavor changing neutral currents(FCNC's) are absent if one introduces an *ad hoc* discrete symmetry to constrain the 2HDM scalar potential and Yukawa Lagrangian. Lets consider a Yukawa Lagrangian of the form [38]

$$\mathcal{L}_Y = \eta_{ij}^U \bar{Q}_{i,L} \tilde{\phi}_1 U_{j,R} + \eta_{ij}^D \bar{Q}_{i,L} \phi_1 D_{j,R} + \xi_{ij}^U \bar{Q}_{i,L} \tilde{\phi}_2 U_{j,R} + \xi_{ij}^D \bar{Q}_{i,L} \phi_2 D_{j,R} + h.c., \quad (1)$$

where ϕ_i ($i = 1, 2$) are the two Higgs doublets of a two-Higgs-doublet model, $\tilde{\phi}_{1,2} = i\tau_2 \phi_{1,2}^*$, $Q_{i,L}$ ($U_{j,R}$) with $i = (1, 2, 3)$ are the left-handed isodoublet quarks (right-handed up-type quarks), $D_{j,R}$ are the right-handed isosinglet down-type quarks, while $\eta_{i,j}^{U,D}$ and $\xi_{i,j}^{U,D}$ ($i, j = 1, 2, 3$ are family index) are generally the nondiagonal matrices of the Yukawa coupling. By imposing the discrete symmetry

$$\phi_1 \rightarrow -\phi_1, \phi_2 \rightarrow \phi_2, D_i \rightarrow -D_i, U_i \rightarrow \mp U_i \quad (2)$$

one obtains the so called models I and model II. In model I the third and fourth term in Eq.(1) will be dropped by the discrete symmetry, therefore, both the up- and down-type quarks get mass from Yukawa couplings to the same Higgs doublet ϕ_1 , while the ϕ_2 has no Yukawa couplings to the quarks. For model II, on the other hand, the first and fourth term in Eq.(1) will be dropped by imposing the discrete symmetry. Model II has, consequently the up- and down-type quarks getting mass from Yukawa couplings to two different scalar doublets ϕ_1 and ϕ_2 .

During past years, models I and II have been studied extensively in literature and tested experimentally, and the model II has been very popular since it is the building block of the minimal supersymmetric standard model. In this paper, we focus on the third type of the two-Higgs-doublet model [39], usually known as the model III [38,39]. In model III, no discrete symmetry is imposed and both up- and down-type quarks then may have diagonal and/or flavor changing couplings with ϕ_1 and ϕ_2 . As described in Ref. [38], one can choose a suitable basis (H^0, H^1, H^2, H^\pm) to express two Higgs doublets [38]

$$\phi_1 = \frac{1}{\sqrt{2}} \begin{pmatrix} \sqrt{2}\chi^+ \\ v + H^0 + i\chi^0 \end{pmatrix}, \quad \phi_2 = \frac{1}{\sqrt{2}} \begin{pmatrix} \sqrt{2}H^+ \\ H^1 + iH^2 \end{pmatrix}, \quad (3)$$

and take their vacuum expectation values as the form

$$\langle \phi_1 \rangle = \begin{pmatrix} 0 \\ v/\sqrt{2} \end{pmatrix}, \quad \langle \phi_2 \rangle = 0, \quad (4)$$

where $v = (\sqrt{2}G_F)^{-1/2} = 246\text{GeV}$. The transformation relation between (H^0, H^1, H^2) and the mass eigenstates (\bar{H}^0, h^0, A^0) can be found in Ref. [38]. The H^\pm are the physical charged Higgs boson, H^0 and h^0 are the physical CP-even neutral Higgs boson and the A^0 is the physical CP-odd neutral Higgs boson. After the rotation of quark fields, the Yukawa Lagrangian of quarks are of the form [38],

$$\mathcal{L}_Y^{III} = \eta_{ij}^U \bar{Q}_{i,L} \tilde{\phi}_1 U_{j,R} + \eta_{ij}^D \bar{Q}_{i,L} \phi_1 D_{j,R} + \hat{\xi}_{ij}^U \bar{Q}_{i,L} \tilde{\phi}_2 U_{j,R} + \hat{\xi}_{ij}^D \bar{Q}_{i,L} \phi_2 D_{j,R} + H.c., \quad (5)$$

where $\eta_{ij}^{U,D}$ correspond to the diagonal mass matrices of up- and down-type quarks, while the neutral and charged flavor changing couplings will be [38]²

$$\xi_{ij}^{U,D} = \frac{\sqrt{m_i m_j}}{v} \lambda_{ij}, \quad \hat{\xi}_{neutral}^{U,D} = \xi^{U,D}, \quad \hat{\xi}_{charged}^U = \xi^U V_{CKM}, \quad \hat{\xi}_{charged}^D = V_{CKM} \xi^D, \quad (6)$$

where V_{CKM} is the Cabibbo-Kabayashi-Maskawa mixing matrix [40], $i, j = (1, 2, 3)$ are the generation index. The coupling constants λ_{ij} are free parameters to be determined by experiments, and they may also be complex.

In model II and assuming $\tan \beta \geq 1$, the constraint on the mass of charged Higgs boson due to CLEO data of $b \rightarrow s\gamma$ is $M_{H^+} \geq 200$ GeV at the NLO level [41]. For model I, however, the limit can be much weaker due to the possible destructive interference with the SM amplitude.

For model III, the situation is not as clear as model II because there are more free parameters here. As pointed in Ref. [38], the data of $K^0 - \bar{K}^0$ and $B_d^0 - \bar{B}_d^0$ mixing processes put severe constraint on the FC couplings involving the first generation of quarks. Imposing the limit $\lambda_{1j} = 0$ for $j = (1, 2, 3)$ and assuming all other λ_{ij} parameters are of order 1, Atwood *et al.* [42] found a very strong constraint of $M_{H^+} > 600$ GeV by using the CLEO data of $b \rightarrow s\gamma$ decay available in 1995. But this constraint will be lowered to $M_{H^+} \geq 400$ GeV by using the new CLEO data of $b \rightarrow s\gamma$ decay [35]. In Ref. [43], Aliev *et al.* studied the $b \rightarrow s\gamma$ decay in model III by extending the NLO results of model II [41] to the case of model III, and found some constraints on the FC couplings.

In a recent paper [44], Chao *et al.* studied the decay $b \rightarrow s\gamma$ by assuming that only the couplings $\lambda_{tt} = |\lambda_{tt}|e^{i\theta_t}$ and $\lambda_{bb} = |\lambda_{bb}|e^{i\theta_b}$ are non-zero. They found that the constraint on M_{H^+} imposed by the CLEO data of $b \rightarrow s\gamma$ can be greatly relaxed by considering the phase effects of λ_{tt} and λ_{bb} . From the studies of refs. [35,44], we know that for model III the parameter space

$$\begin{aligned} \lambda_{ij} &= 0, \quad \text{for } ij \neq tt, \text{ or } bb, \\ |\lambda_{tt}| &= 0.3, \quad |\lambda_{bb}| = 35, \quad \theta = (0^\circ - 30^\circ), \quad M_{H^+} = (200 \pm 100)\text{GeV}, \end{aligned} \quad (7)$$

are allowed by the available data, where $\theta = \theta_{bb} - \theta_{tt}$. For the mass M_{H^+} , searches for pair production at LEP have excluded masses $M_{H^+} \leq 77$ GeV [45]. Combining the direct and indirect limits together, we here conservatively consider the range of $100\text{GeV} \leq M_{H^+} \leq 300$ GeV, while take $M_{H^+} = 200$ GeV as the typical value for models I, II and III. For models I and II we consider the range of $1 \leq \tan \beta \leq 30$, while take $\tan \beta = 2$ as the typical value. In the following sections, we will calculate the new physics contributions to the exclusive two-body charmless decays of B meson in the Chao-Cheung-Keung (CCK) scenario of model III [44]. Model III in the CCK scenario has following advantages:

1. Since we keep only the couplings λ_{tt} and λ_{bb} none zero, the neutral Higgs bosons do not contribute at tree level or one-loop level. The new contributions therefore come only from the charged Higgs penguin diagrams with the heavy internal top quark.

²We make the same ansatz on the $\xi_{ij}^{U,D}$ couplings as the Ref. [38]. For more details about the definition of $\hat{\xi}^{U,D}$ one can see Ref. [38].

2. The new operators $O_{9,10}$ and all flipped chirality partners of operators $O_{1,\dots,10}$ as defined in Ref. [43] do not contribute to the decay $b \rightarrow s\gamma$ and the exclusive two-body charmless hadronic B decays under study in this paper.
3. The free parameters are greatly reduced to λ_{tt} , λ_{bb} and M_{H^+} in model III, and $\tan\beta$ and M_{H^+} in models I and II.

III. EFFECTIVE WILSON COEFFICIENTS IN SM AND 2HDM'S

In this section we evaluate the new gluonic and electroweak penguin diagrams and present the well-known effective Hamiltonian for the two-body charmless decays $B \rightarrow h_1 h_2$ with the inclusion of new physics contributions. For more details about the effective Hamiltonian with generalized factorization for B decays one can see, for example, Refs. [7,9].

A. Operators and Wilson coefficients

The standard theoretical frame to calculate the inclusive three-body decays $b \rightarrow s\bar{q}q$ ³ is based on the effective Hamiltonian [12,7],

$$\mathcal{H}_{eff}(\Delta B = 1) = \frac{G_F}{\sqrt{2}} \left\{ \sum_{j=1}^2 C_j (V_{ub}V_{us}^* Q_j^u + V_{cb}V_{cs}^* Q_j^c) - V_{tb}V_{ts}^* \left[\sum_{j=3}^{10} C_j Q_j + C_g Q_g \right] \right\} \quad (8)$$

where C_j and C_g are Wilson coefficients, and the operator basis reads:

$$Q_1 = (\bar{s}q)_{V-A}(\bar{q}b)_{V-A}, \quad Q_2 = (\bar{s}_\alpha q_\beta)_{V-A}(\bar{q}_\beta b_\alpha)_{V-A}, \quad (9)$$

with $q = u$ and $q = c$, and

$$Q_3 = (\bar{s}b)_{V-A} \sum_{q'} (\bar{q}'q')_{V-A}, \quad Q_4 = (\bar{s}_\alpha b_\beta)_{V-A} \sum_{q'} (\bar{q}'_\beta q'_\alpha)_{V-A}, \quad (10)$$

$$Q_5 = (\bar{s}b)_{V-A} \sum_{q'} (\bar{q}'q')_{V+A}, \quad Q_6 = (\bar{s}_\alpha b_\beta)_{V-A} \sum_{q'} (\bar{q}'_\beta q'_\alpha)_{V+A}, \quad (11)$$

$$Q_7 = \frac{3}{2}(\bar{s}b)_{V-A} \sum_{q'} e_{q'} (\bar{q}'q')_{V+A}, \quad Q_8 = \frac{3}{2}(\bar{s}_\alpha b_\beta)_{V-A} \sum_{q'} e_{q'} (\bar{q}'_\beta q'_\alpha)_{V+A}, \quad (12)$$

$$Q_9 = \frac{3}{2}(\bar{s}b)_{V-A} \sum_{q'} e_{q'} (\bar{q}'q')_{V-A}, \quad Q_{10} = \frac{3}{2}(\bar{s}_\alpha b_\beta)_{V-A} \sum_{q'} e_{q'} (\bar{q}'_\beta q'_\alpha)_{V-A}, \quad (13)$$

$$Q_g = \frac{g_s}{8\pi^2} m_b \bar{s}_\alpha \sigma^{\mu\nu} (1 + \gamma_5) T_{\alpha\beta}^a b_\beta G_{\mu\nu}^a \quad (14)$$

where α and β are the $SU(3)$ color indices, $T_{\alpha\beta}^a$ ($a = 1, \dots, 8$) are the Gell-Mann matrices. The sum over q' runs over the quark fields that are active at the scale $\mu = O(m_b)$, i.e., $q' \in \{u, d, s, c, b\}$. Q_1 and Q_2 are current-current operators, $Q_{3,4,5,6}$ and $Q_{7,8,9,10}$ are QCD

³For $b \rightarrow d\bar{q}q$ decays, one simply make the replacement $s \rightarrow d$.

and electroweak penguin operators, and Q_g is the chromo-magnetic dipole (CMD) operator. Following Ref. [7], we also neglect the effects of the electromagnetic penguin operator $Q_{7\gamma}$, and do not consider the effect of the weak annihilation and exchange diagrams.

In the SM, the Wilson coefficients $C_1(M_W), \dots, C_{10}(M_W)$ at NLO level and $C_g(M_W)$ at leading order (LO) have been given for example in Refs. [11,12]. They read in the naive dimensional regularization (NDR) scheme

$$\begin{aligned}
C_1(M_W) &= 1 - \frac{11}{6} \frac{\alpha_s(M_W)}{4\pi} - \frac{35}{18} \frac{\alpha_{em}}{4\pi}, \\
C_2(M_W) &= \frac{11}{2} \frac{\alpha_s(M_W)}{4\pi}, \\
C_3(M_W) &= -\frac{\alpha_s(M_W)}{24\pi} \left[E_0(x_t) - \frac{2}{3} \right] + \frac{\alpha_{em}}{6\pi} \frac{1}{\sin^2 \theta_W} [2B_0(x_t) + C_0(x_t)], \\
C_4(M_W) &= \frac{\alpha_s(M_W)}{8\pi} \left[E_0(x_t) - \frac{2}{3} \right], \\
C_5(M_W) &= -\frac{\alpha_s(M_W)}{24\pi} \left[E_0(x_t) - \frac{2}{3} \right], \\
C_6(M_W) &= \frac{\alpha_s(M_W)}{8\pi} \left[E_0(x_t) - \frac{2}{3} \right], \\
C_7(M_W) &= \frac{\alpha_{em}}{6\pi} \left[4C_0(x_t) + D_0(x_t) - \frac{4}{9} \right], \\
C_8(M_W) &= 0, \\
C_9(M_W) &= \frac{\alpha_{em}}{6\pi} \left[4C_0(x_t) + D_0(x_t) - \frac{4}{9} + \frac{1}{\sin^2 \theta_W} (10B_0(x_t) - 4C_0(x_t)) \right], \\
C_{10}(M_W) &= 0, \\
C_g(M_W) &= -\frac{E'_0(x_t)}{2},
\end{aligned} \tag{15}$$

where $x_t = m_t^2/M_W^2$, the functions $B_0(x)$, $C_0(x)$, $D_0(x)$, $E_0(x)$ and E'_0 are the familiar Inami-Lim functions [46],

$$B_0(x) = \frac{1}{4} \left[\frac{x}{1-x} + \frac{x \ln x}{(x-1)^2} \right], \tag{17}$$

$$C_0(x) = \frac{x}{8} \left[\frac{x-6}{x-1} + \frac{3x+2}{(x-1)^2} \ln x \right], \tag{18}$$

$$D_0(x) = -\frac{4}{9} \ln x + \frac{-19x^3 + 25x^2}{36(x-1)^3} + \frac{x^2(5x^2 - 2x - 6)}{18(x-1)^4} \ln x, \tag{19}$$

$$E_0(x) = \frac{18x - 11x^2 - x^3}{12(1-x)^3} - \frac{4 - 16x + 9x^2}{6(1-x)^4} \ln[x], \tag{20}$$

$$E'_0(x) = \left[\frac{2x + 5x^2 - x^3}{4(1-x)^3} + \frac{3x^2}{2(1-x)^4} \log[x] \right]. \tag{21}$$

Here function $B_0(x)$ results from the evaluation of the box diagrams with leaving lepton pair $\nu\bar{\nu}$ or l^+l^- [12], function $C_0(x)$ from the Z^0 -penguin, function $D_0(x)$ and $E_0(x)$ from the photon penguin and the gluon penguin diagram respectively, and finally function $E'_0(x)$ arise from the magnetic gluon penguin.

B. Contributions of charged-Higgs penguin diagrams

For the charmless hadronic decays of B meson under consideration, the new physics will manifest itself by modifying the corresponding Inami-Lim functions $C_0(x)$, $D_0(x)$, $E_0(x)$ and $E'_0(x)$ which determine the coefficients $C_3(M_W), \dots, C_{10}(M_W)$ and $C_g(M_W)$. These modifications, in turn, will change for example the standard model predictions for the branching ratios for decays $B \rightarrow h_1 h_2$. The new strong and electroweak penguin diagrams can be obtained from the corresponding penguin diagrams in the SM by replacing the internal W^\pm lines with the charged-Higgs H^\pm lines, as shown in Fig.1. In the analytical calculations of those penguin diagrams, we will use dimensional regularization to regulate all the ultraviolet divergences in the virtual loop corrections and adopt the \overline{MS} renormalization scheme. It is easy to show that all ultraviolet divergences are canceled after summing up all Feynman diagrams.

By evaluating analytically the new Z^0 -, γ - and gluonic penguins induced by the exchanges of charged-Higgs boson H^\pm in the model III, we find the new C_0 , D_0 , E_0 and E'_0 functions,

$$C_0^{III} = \frac{-x_t}{16} \left[\frac{y_t}{1-y_t} + \frac{y_t}{(1-y_t)^2} \ln[y_t] \right] \cdot |\lambda_{tt}|^2, \quad (22)$$

$$D_0^{III} = -\frac{1}{3} H(y_t) |\lambda_{tt}|^2, \quad (23)$$

$$E_0^{III} = -\frac{1}{2} I(y_t) |\lambda_{tt}|^2, \quad (24)$$

$$E'_0{}^{III} = \frac{1}{6} J(y_t) |\lambda_{tt}|^2 - K(y_t) |\lambda_{tt} \lambda_{bb}| e^{i\theta}, \quad (25)$$

with

$$H(y) = \frac{38y - 79y^2 + 47y^3}{72(1-y)^3} + \frac{4y - 6y^2 + 3y^4}{12(1-y)^4} \ln[y], \quad (26)$$

$$I(y) = \frac{16y - 29y^2 + 7y^3}{36(1-y)^3} + \frac{2y - 3y^2}{6(1-y)^4} \log[y], \quad (27)$$

$$J(y) = \frac{2y + 5y^2 - y^3}{4(1-y)^3} + \frac{3y^2}{2(1-y)^4} \log[y], \quad (28)$$

$$K(y) = \frac{-3y + y^2}{4(1-y)^2} - \frac{y}{2(1-y)^3} \log[y], \quad (29)$$

where $x_t = m_t^2/M_W^2$, $y_t = m_t^2/M_{H^\pm}^2$, and the small terms proportional to m_b^2/m_t^2 have been neglected.

In models I and II, one can find the corresponding functions C_0 , D_0, E_0 and E'_0 by evaluating the new strong and electroweak penguins in the same way as in model III

$$C_0^I = C_0^{II} = \frac{-x_t}{8 \tan^2 \beta} \left[\frac{y_t}{1-y_t} + \frac{y_t}{(1-y_t)^2} \ln[y_t] \right], \quad (30)$$

$$D_0^I = D_0^{II} = -\frac{2}{3 \tan^2 \beta} H(y_t), \quad (31)$$

$$E_0^I = E_0^{II} = \frac{1}{\tan^2 \beta} I(y_t), \quad (32)$$

$$E_0'^I = \frac{1}{3 \tan^2 \beta} [J(y_t) - 6K(y_t)] , \quad (33)$$

$$E_0'^{II} = \frac{1}{3 \tan^2 \beta} J(y_t) + 2K(y_t) , \quad (34)$$

where $y_t = m_t^2/M_{H^+}^2$, $\tan \beta = v_2/v_1$ where v_1 and v_2 are the vacuum expectation values of the Higgs doublet ϕ_1 and ϕ_2 .

We combine the SM part and the new physics part of the corresponding functions to define the functions at the scale $\mu = M_W$ as follows

$$F_0(M_W) = F_0^{SM} + F_0^{NP} , \quad (35)$$

where $F_0 \in \{C_0, D_0, E_0, E_0'\}$.

Since the heavy new particles appeared in the 2HDM's have been integrated out at the scale M_W , the QCD running of the Wilson coefficients $C_i(M_W)$ down to the scale $\mu = O(m_b)$ after including the NP contributions will be the same as in the SM. By using QCD renormalization group equations [11,12], it is straightforward to run Wilson coefficients $C_i(M_W)$ from the scale $\mu = 0(M_W)$ down to the lower scale $\mu = O(m_b)$. Working consistently to the NLO precision, the Wilson coefficients C_i for $i = 1, \dots, 10$ are needed in NLO precision, while it is sufficient to use the leading logarithmic value for C_g :

$$\mathbf{C}(\mu) = U(\mu, M_W) \mathbf{C}(M_W) , \quad (36)$$

$$C_g(\mu) = \eta^{14/23} C_g(M_W) + \sum_{i=1}^8 \bar{h}_i \eta^{a_i} , \quad (37)$$

where $\mathbf{C}(M_W) = (C_1(M_W), \dots, C_{10}(M_W))^T$, $U(\mu, M_W)$ is the five-flavor 10×10 evolution matrix at NLO level as defined in Ref. [11], $\eta = \alpha_s(M_W)/\alpha_s(\mu)$, and the constants \bar{h}_i and a_i can also be found in Ref. [11].

At NLO level, the Wilson coefficients are usually renormalization scheme(RS) dependent. In the NDR scheme, by using the input parameters as given in Appendix and Eq.(7), and setting $M_{H^+} = 200$ GeV, $\theta = 0^0$, $\tan \beta = 2$ and $\mu = 2.5$ GeV, we find the Wilson coefficients $C_g^{eff}(\mu) = C_g + C_5$ and $C_i(\mu)$ with $i = 1, \dots, 10$ in the SM and models I, II and III, and list them in Table I. From the numerical results as listed in Table I, one can easily see that:

- The values of $C_i(\mu)$ ($i = 1, \dots, 10$) in models I, II and III are almost identical with those in the SM. Only the coefficient C_g^{eff} in models II and III are clearly different from that in the SM.
- It is the coefficient C_g^{eff} partially induced by the new gluonic penguin diagrams which will dominate the total new physics corrections to the decay processes under study.

C. Effective Wilson coefficients

We know that the unphysical RS dependence of Wilson coefficients will be cancelled by the corresponding dependence in the matrix elements of the operators in \mathcal{H}_{eff} , as shown explicitly in Refs. [12,47]. Very recently, Cheng *et al.* [18] studied and resolved the so-called

gauge and infrared problems [17] of generalized factorization approach ⁴. They found that the gauge invariance is maintained under radiative corrections by working in the physical on-mass-shell scheme, while the infrared divergence in radiative corrections should be isolated using the dimensional regularization and the resultant infrared poles are absorbed into the universal meson wave functions [18].

The one-loop matrix elements can be rewritten in terms of the tree-level matrix elements of the effective operators [7]

$$\langle sq'\bar{q}'|\mathcal{H}_{eff}|b\rangle = \sum_{i,j} C_i^{eff}(\mu) \langle sq'\bar{q}'|O_j|b\rangle^{\text{tree}}. \quad (38)$$

where $C_i^{eff}(\mu)$ ($i = 1, \dots, 10$) are the effective Wilson coefficients. In the NDR scheme and for $SU(3)_C$, the effective Wilson coefficients C_i^{eff} can be written as [7,9],

$$C_i^{eff} = \left[1 + \frac{\alpha_s}{4\pi} \left(r_V^T + \gamma_V^T \log \frac{m_b}{\mu} \right) \right]_{ij} C_j + \frac{\alpha_s}{24\pi} A'_i (C_t + C_p + C_g) + \frac{\alpha_{ew}}{8\pi} B'_i C_e, \quad (39)$$

where $A'_i = (0, 0, -1, 3, -1, 3, 0, 0, 0, 0)^T$, $B'_i = (0, 0, 0, 0, 0, 0, 1, 0, 1, 0)^T$, the matrices \hat{r}_V and γ_V contain the process-independent contributions from the vertex diagrams. Like ref. [9], we here include vertex corrections to $C_7 - C_{10}$ ⁵. The anomalous dimension matrix γ_V has been given explicitly, for example, in Eq.(2.17) of Ref. [9]. Note that the correct value of the element $(\hat{r}_{NDR})_{66}$ and $(\hat{r}_{NDR})_{88}$ should be 17 instead of 1 as pointed in Ref. [48], \hat{r}_V in the NDR scheme takes the form

$$\hat{r}_V^{NDR} = \begin{pmatrix} 3 & -9 & 0 & 0 & 0 & 0 & 0 & 0 & 0 & 0 \\ -9 & 3 & 0 & 0 & 0 & 0 & 0 & 0 & 0 & 0 \\ 0 & 0 & 3 & -9 & 0 & 0 & 0 & 0 & 0 & 0 \\ 0 & 0 & -9 & 3 & 0 & 0 & 0 & 0 & 0 & 0 \\ 0 & 0 & 0 & 0 & -1 & 3 & 0 & 0 & 0 & 0 \\ 0 & 0 & 0 & 0 & -3 & 17 & 0 & 0 & 0 & 0 \\ 0 & 0 & 0 & 0 & 0 & 0 & -1 & 3 & 0 & 0 \\ 0 & 0 & 0 & 0 & 0 & 0 & -3 & 17 & 0 & 0 \\ 0 & 0 & 0 & 0 & 0 & 0 & 0 & 0 & 3 & -9 \\ 0 & 0 & 0 & 0 & 0 & 0 & 0 & 0 & -9 & 3 \end{pmatrix}. \quad (40)$$

The function C_t , C_p , and C_g describe the penguin-type corrections to the operators $Q_{1,2}$, $Q_{3,\dots,6}$, and the tree-level diagram of the operator Q_g respectively. We here follow the procedure of Ref. [15] to include C_g in (39). The effective Wilson coefficients C_i^{eff} in Eq.(39) are now scheme and scale independent in NLO precision, and also gauge invariant and infrared safe. The explicit expressions of functions C_t , C_p , and C_g in the NDR scheme have been given, for example, in Refs. [7,9]

⁴The reliability of the generalized factorization approach is improved by this progress.

⁵Numerically, such corrections are negligibly small.

$$C_t = \left[\frac{2}{3} + \frac{\lambda_u}{\lambda_t} G(m_u) + \frac{\lambda_c}{\lambda_t} G(m_c) \right] C_1, \quad (41)$$

$$C_p = \left[\frac{4}{3} - G(m_q) - G(m_b) \right] C_3 + \sum_{i=u,d,s,c,b} \left[\frac{2}{3} - G(m_i) \right] (C_4 + C_6), \quad (42)$$

$$C_e = \frac{8}{9} \left[\frac{2}{3} + \frac{\lambda_u}{\lambda_t} G(m_u) + \frac{\lambda_c}{\lambda_t} G(m_c) \right] (C_1 + 3C_2), \quad (43)$$

$$C_g = -\frac{2m_b}{\sqrt{\langle k^2 \rangle}} C_g^{\text{eff}}, \quad (44)$$

with $\lambda_{q'} \equiv V_{q'b} V_{q'q}^*$. The function $G(m)$ is of the form [49]

$$G(m) = \frac{10}{9} - \frac{2}{3} \ln\left[\frac{m^2}{\mu^2}\right] + \frac{2\mu^2}{3m^2} - \frac{2(1+2z)}{3z} g(z) \quad (45)$$

where $z = k^2/(4m^2)$, and

$$g(z) = \begin{cases} \sqrt{\frac{1-z}{z}} \arctan\left[\frac{z}{1-z}\right], & z < 1, \\ \sqrt{\frac{1-z}{4z}} \left[\ln\left[\frac{\sqrt{z}+\sqrt{z-1}}{\sqrt{z}-\sqrt{z-1}}\right] - i\pi \right], & z > 1. \end{cases} \quad (46)$$

where k^2 is the momentum squared transferred by the virtual gluon, photon or Z to the $q'\bar{q}'$ pair in inclusive three-body decays $b \rightarrow qq'\bar{q}'$, and m is the mass of internal up-type quark in the penguin diagrams. For $k^2 > 4m^2$, an imaginary part of $g(z)$ will appear because of the generation of a strong phase at the $\bar{u}u$ and $\bar{c}c$ threshold [49–51].

For the two-body exclusive B meson decays any information on k^2 is lost in the factorization assumption, and it is not clear what “relevant” k^2 should be taken in numerical calculation. One usually uses the “physical” range for k^2 : $m_b^2/4 \lesssim k^2 \lesssim m_b^2/2$. Following Refs. [7,9], we also use $k^2 = m_b^2/2$ in the numerical calculation and will consider the k^2 -dependence of branching ratios of charmless B meson decays for several typical decay channels.

IV. DECAY AMPLITUDES IN BSW MODEL

In numerical calculations, two sets of form factors at the zero momentum transfer from the Baner, Stech and Wirbel (BSW) model [13], as well as Lattice QCD and Light-cone QCD sum rules (LQCSR) [52] will be used respectively. Explicit values of these form factors can be found in [7] and have also been given in Appendix. Following Ref. [7], the seventy six decay channels of B_u and B_d mesons are classified into five classes according to their N^{eff} -dependence:

- Class-I: including four decay modes, $B^0 \rightarrow \pi^- \pi^+, \rho^\pm \pi^\mp$ and $B^0 \rightarrow \rho^- K^+$, the large and N^{eff} stable coefficient a_1 play the major role.
- Class-II: including ten decay modes, for example $B^0 \rightarrow \pi^0 \pi^0$, and the relevant coefficient for these decays is a_2 which shows a strong N^{eff} -dependence.

- Class-III: including nine decay modes involving the interference of class-I and class-II decays, such as the decays $B^+ \rightarrow \pi^+ \eta'$.
- Class-IV: including twenty two $B \rightarrow h_1 h_2$ decay modes such as $B \rightarrow K \eta^{(\prime)}$ decays. The amplitudes of these decays involve one (or more) of the dominant penguin coefficients $a_{4,6,9}$ with constructive interference among them. The Class-IV decays are N^{eff} stable.
- Class-V: including twelve $B \rightarrow h_1 h_2$ decay modes, such as $B \rightarrow \pi^0 \eta^{(\prime)}$ and $B \rightarrow \phi K$ decays. Since the amplitudes of these decays involve large and delicate cancellations due to interference between strong N^{eff} -dependent coefficients $a_{3,5,7,10}$ and the dominant penguin coefficients $a_{4,6,9}$, these decays are generally not stable against N^{eff} .

With the factorization ansatz [13,53,54], the three-hadron matrix elements or the decay amplitude $\langle XY|H_{eff}|B \rangle$ can be factorized into a sum of products of two current matrix elements $\langle X|J_1^\mu|0 \rangle$ and $\langle Y|J_{2\mu}|B \rangle$ (or $\langle Y|J_1^\mu|0 \rangle$ and $\langle X|J_{2\mu}|B \rangle$). The former matrix elements are of the form [55]

$$\begin{aligned} \langle 0|J_\mu|X(0^-) \rangle &= i f_X k_\mu, \\ \langle 0|\bar{q}_1 \gamma_\mu q_2|X(1^-) \rangle &= g_X M_X \epsilon_\mu, \\ \langle 0|\bar{q}_1 \gamma_\mu \gamma_5 q_2|X(1^-) \rangle &= 0, \end{aligned} \quad (47)$$

where f_X and g_X are the decay constant of pseudoscalar and vector mesons, ϵ_μ is the polarization vector of the vector meson. For the second matrix element $\langle Y|J_{2\mu}|B \rangle$, the expression in terms of Lorentz-scalar form factors $A_{0,1,2}(k^2)$ and $F_{0,1}(k^2)$ [13,55], are of the form

$$\begin{aligned} \langle X(0^-)|J_\mu|B \rangle &= \left[(p_B + p_X)_\mu - \frac{M_B^2 - M_X^2}{k^2} k_\mu \right] F_1^{B \rightarrow X}(k^2) \\ &\quad + \frac{M_B^2 - M_X^2}{k^2} k_\mu F_0^{B \rightarrow X}(k^2), \end{aligned} \quad (48)$$

$$\begin{aligned} \langle X(1^-)|J_\mu|B \rangle &= \frac{2}{M_B + M_X} \epsilon_{\mu\nu\rho\sigma} \epsilon^{*\nu} p_B^\rho p_X^\sigma V^{B \rightarrow X}(k^2) + i \epsilon^* \cdot k \frac{2M_X}{k^2} k_\mu A_0(k^2) \\ &\quad + i (M_B + M_X) \left[\epsilon_\mu^* - \frac{\epsilon^* \cdot k}{k^2} k_\mu \right] A_1(k^2) \\ &\quad - i \frac{\epsilon^* \cdot k}{M_B + M_X} \left[(p_B + p_X)_\mu - \frac{M_B^2 - M_X^2}{k^2} k_\mu \right] A_2(k^2), \end{aligned} \quad (49)$$

where $k = p_B - p_X$, and M_B, M_X, M_Y are the masses of B meson and the daughter meson X and Y, respectively. The explicit expressions of form factors $F_{0,1}(k^2), V(k^2)$ and $A_{0,1,2}(k^2)$ have been given in Appendix.

In the B rest frame, the branching ratios of two-body B meson decays can be written as

$$\mathcal{B}(B \rightarrow XY) = \tau_B \frac{|p|}{8\pi M_B^2} |M(B \rightarrow XY)|^2 \quad (50)$$

for $B \rightarrow PP$ decays, and

$$\mathcal{B}(B \rightarrow XY) = \tau_B \frac{|p|^3}{8\pi M_V^2} |M(B \rightarrow XY)/(\epsilon \cdot p_B)|^2 \quad (51)$$

for $B \rightarrow PV$ decays. Here $\tau(B_u^-) = 1.65ps$ and $\tau(B_d^0) = 1.56ps$ [56], p_B is the four-momentum of the B meson, M_V and ϵ is the mass and polarization vector of the produced light vector meson respectively, and $|p|$ is the magnitude of momentum of particle X and Y in the B rest frame,

$$|p| = \frac{1}{2M_B} \sqrt{[M_B^2 - (M_X + M_Y)^2][M_B^2 - (M_X - M_Y)^2]} \quad (52)$$

For $B \rightarrow VV$ decays, one needs to evaluate the helicity matrix element $H_\lambda = \langle V_1(\lambda)V_2(\lambda)|H_{eff}|B \rangle$ with $\lambda = 0, \pm 1$. The branching ratio of the decay $B \rightarrow V_1V_2$ is given in terms of H_λ by

$$\mathcal{B}(B \rightarrow V_1V_2) = \tau_B \frac{|p|}{8\pi M_B^2} (|H_0|^2 + |H_{+1}|^2 + |H_{-1}|^2) \quad (53)$$

where $|p|$ has been given in Eq.(52). The three independent helicity amplitudes H_0 , H_{+1} and H_{-1} can be expressed by three invariant amplitudes a, b, c defined by the decomposition

$$H_\lambda = i\epsilon^\mu(\lambda)\eta^\nu(\lambda) \left[ag_{\mu\nu} + \frac{b}{M_1M_2} p_\mu p_\nu + \frac{ic}{M_1M_2} \epsilon_{\mu\nu\alpha\beta} p_1^\alpha p_2^\beta \right] \quad (54)$$

where $p_{1,2}$ and $M_{1,2}$ are the four momentum and masses of $V_{1,2}$, respectively. $p = p_1 + p_2$ is the four-momentum of B meson, and

$$H_{\pm 1} = a \pm c\sqrt{x^2 - 1}, \quad H_0 = -ax - b(x^2 - 1) \quad (55)$$

$$x = \frac{M_B^2 - M_1^2 - M_2^2}{2M_1M_2} \quad (56)$$

For individual decay mode, the coefficients a, b and c can be determined by comparing the helicity amplitude $H_\lambda = \langle V_1(\lambda)V_2(\lambda)|H_{eff}|B \rangle$ with the expression (54).

In the generalized factorization ansatz, the effective Wilson coefficients C_i^{eff} will appear in the decay amplitudes in the combinations:

$$a_{2i-1} \equiv C_{2i-1}^{eff} + \frac{C_{2i}^{eff}}{N^{eff}}, \quad a_{2i} \equiv C_{2i}^{eff} + \frac{C_{2i-1}^{eff}}{N^{eff}}, \quad (i = 1, \dots, 5) \quad (57)$$

where the effective number of colors N^{eff} is treated as a free parameter varying in the range of $2 \leq N^{eff} \leq \infty$, in order to model the nonfactorizable contribution to the hadronic matrix elements. It is evident that the reliability of generalized factorization approach has been improved since the effective Wilson coefficients C_i^{eff} appeared in Eq.(57) are now gauge invariant and infrared safe. Although N^{eff} can in principle vary from channel to channel, but in the energetic two-body hadronic B meson decays, it is expected to be process insensitive as supported by the data [9]. As argued in ref. [14], $N^{eff}(LL)$ induced by the $(V-A)(V-A)$ operators can be rather different from $N^{eff}(LR)$ generated by $(V-A)(V+A)$ operators. In this paper, however, we will simply assume that $N^{eff}(LL) \equiv N^{eff}(LR) = N^{eff}$ and consider

the variation of N^{eff} in the range of $2 \leq N^{eff} \leq \infty$ since we here focus on the calculation of new physics effects on the studied B meson decays induced by the new penguin diagrams in the two-Higgs-doublet models. For more details about the cases of $N^{eff}(LL) \neq N^{eff}(LR)$, one can see for example ref. [9]. We here will also not consider the possible effects of final state interaction (FSI) and the contributions from annihilation channels although they may play a significant rule for some $B \rightarrow PV, VV$ decays.

Using the input parameters as given in Appendix, and assuming $k^2 = m_b^2/2$, $M_{H^+} = 200$ GeV, $\theta = 0^0$ and $\tan\beta = 2$, the theoretical predictions of effective coefficients a_i are calculated and displayed in Table II and Table III for the transitions $b \rightarrow d$ ($\bar{b} \rightarrow \bar{d}$) and $b \rightarrow s$ ($\bar{b} \rightarrow \bar{s}$), respectively. For coefficients a_3, \dots, a_{10} , the first, second and third entries in tables (II,III) refer to the values of a_i in the SM and models II and III, respectively. a_i in model I are very similar with those in the SM and hence was not given explicitly.

All branching ratios in following three sections are the averages of the branching ratios of B and anti- B decays. The ratio $\delta\mathcal{B}$ describes the magnitude of new physics corrections on the SM prediction of the decay ratios and is defined as

$$\delta\mathcal{B}(B \rightarrow XY) = \frac{\mathcal{B}(B \rightarrow XY)^{2HDM} - \mathcal{B}(B \rightarrow XY)^{SM}}{\mathcal{B}(B \rightarrow XY)^{SM}} \quad (58)$$

V. $B \rightarrow PP$ DECAYS

Using formulae given in last section, it is straightforward to find the decay amplitudes of $B \rightarrow PP$ decays. As an example, we present here the decay amplitude $M(B^- \rightarrow \pi^- \pi^0) = \langle \pi^- \pi^0 | H_{eff} | B_u^- \rangle$,

$$\begin{aligned} M(B^- \rightarrow \pi^- \pi^0) = & \frac{G_F}{2} \left\{ V_{ub} V_{ud}^* \left(a_1 M_{uud}^{\pi^- \pi^0} + a_2 M_{duu}^{\pi^- \pi^0} \right) \right. \\ & - V_{tb} V_{td}^* \left[(a_4 + a_{10} + (a_6 + a_8) R_1) M_{duu}^{\pi^- \pi^0} \right. \\ & \left. \left. - \left(a_4 + \frac{3}{2}(a_7 - a_9) - \frac{a_{10}}{2} + (a_6 - \frac{a_8}{2}) R_2 \right) M_{uud}^{\pi^- \pi^0} \right] \right\} \quad (59) \end{aligned}$$

with

$$R_1 = \frac{2m_{\pi^-}^2}{(m_b - m_u)(m_u + m_d)}, \quad (60)$$

$$R_2 = \frac{m_{\pi^0}^2}{m_d(m_b - m_d)}, \quad (61)$$

$$M_{uud}^{\pi^- \pi^0} = -i(m_B^2 - m_{\pi^-}^2) f_\pi F_0^{B \rightarrow \pi}(m_{\pi^0}^2), \quad (62)$$

$$M_{duu}^{\pi^- \pi^0} = -i(m_B^2 - m_{\pi^0}^2) f_\pi F_0^{B \rightarrow \pi}(m_{\pi^-}^2) \quad (63)$$

where f_π is the decay constant of π meson. The form factor $F_0^{B \rightarrow \pi}(m^2)$ can be found in Appendix. Under the approximation of setting $m_u = m_d$ and $m_{\pi^0} = m_{\pi^-}$, the decay amplitude $M(B^- \rightarrow \pi^- \pi^0)$ in Eq.(59) will be reduced to the form as given in Eq.(80) of Ref. [7]. In the following numerical calculations, we use the decay amplitudes as given

in Appendix A of Ref. [7] directly without further discussions about details of individual amplitude.

In tables IV-VI, we present the numerical results of the branching ratios for the twenty $B \rightarrow PP$ decays in the framework of the SM and models I, II and III by using the BSW and LQQSR form factors, respectively. Theoretical predictions are made by using the central values of input parameters as given in Eq.(7) and Appendix, and assuming $M_{H^+} = 200$ GeV, $\theta = 0^0$, $\tan\beta = 2$ and $N^{eff} = 2, 3, \infty$ in the generalized factorization approach. The k^2 -dependence of the branching ratios is small in the range of $k^2 = m_b^2/2 \pm 2 \text{ GeV}^2$ and hence the numerical results are given by fixing $k^2 = m_b^2/2$.

The currently available CLEO data [22–24] are listed in the last column of table IV. From numerical results, we see that:

- For $B \rightarrow K\eta'$ decays, the observed branching ratio are clearly much larger than the SM predictions [25,29]. All other estimated branching ratios in Table IV are, however, consistent with the new CLEO measurements or 90%*C.L.* upper limits.
- In model III, the new physics corrections to most class-II, IV and V decay channels can be rather large and insensitive to the variations of the mass M_{H^+} and the color number N^{eff} : from 20% to 90% *w.r.t* the SM predictions for both cases of $\theta = 0^0, 30^0$. For tree-dominated decay modes $B \rightarrow \pi^+\pi^-, \pi^+\pi^0, \pi^+\eta^{(\prime)}$, the new physics corrections are small in size.
- In models I and II, however, the new physics corrections to all $B \rightarrow PP$ decay modes are small in size within the considered parameter space: less than 3% in the model I, and $\approx (-20 - 0)\%$ in the model II, as shown in Table VI. So small corrections will be masked by other large theoretical uncertainties.
- In model III, the new gluonic penguins will contribute effectively through the mixing of chromo-magnetic operator Q_g with QCD penguin operators $Q_3 - Q_6$. The C_g^{eff} will strongly dominate the new physics contributions to all $B \rightarrow h_1h_2$ decay modes.
- The central values of the branching ratios obtained by using the LQQSR form factors will be increased by about 15% when compared with the results using the BSW form factors, as can be seen from Table IV. We therefore use the BSW form factors only to calculate the new physics effects on the ratios $\mathcal{B}(B \rightarrow h_1h_2)$ and treat the difference induced by using different set of form factors as one kind of theoretical uncertainties.

A. $B \rightarrow \pi\pi, K\pi$ decays

There are so far seven measured branching ratios of $B \rightarrow PP$ decays: one $B \rightarrow \pi^+\pi^-$ decay, four $B \rightarrow K\pi$ and two $B \rightarrow K\eta'$ decays [23,24,26,27]:

$$\mathcal{B}(B \rightarrow \pi^+\pi^-) = \begin{cases} (4.3_{-1.5}^{+1.6} \pm 0.5) \times 10^{-6}, & [\text{CLEO}], \\ (9.3_{-2.1}^{+2.8} \pm 1.2) \times 10^{-6}, & [\text{BaBar}], \end{cases} \quad (64)$$

$$\mathcal{B}(B \rightarrow K^+\pi^0) = \begin{cases} (11.6_{-2.7}^{+3.0} \pm 1.4) \times 10^{-6}, & [\text{CLEO}], \\ (18.8_{-4.9}^{+5.5} \pm 2.3) \times 10^{-6}, & [\text{Belle}], \end{cases} \quad (65)$$

$$\mathcal{B}(B \rightarrow K^+\pi^-) = \begin{cases} (17.2_{-2.4}^{+2.5} \pm 1.2) \times 10^{-6}, & [\text{CLEO}], \\ (12.5_{-2.6}^{+3.0} \pm 2.3) \times 10^{-6}, & [\text{BaBar}], \\ (17.4_{-4.6}^{+5.1} \pm 3.4) \times 10^{-6}, & [\text{Belle}], \end{cases} \quad (66)$$

$$\mathcal{B}(B \rightarrow K^0\pi^+) = (18.2_{-4.0}^{+4.6} \pm 1.6) \times 10^{-6}, \quad [\text{CLEO}], \quad (67)$$

$$\mathcal{B}(B \rightarrow K^0\pi^0) = \begin{cases} (14.6_{-5.1}^{+5.9} \pm 2.4) \times 10^{-6}, & [\text{CLEO}], \\ (21_{-7.8}^{+9.3} \pm 2.5) \times 10^{-6}, & [\text{Belle}], \end{cases} \quad (68)$$

$$\mathcal{B}(B \rightarrow K^+\eta') = \begin{cases} (80_{-9}^{+10} \pm 7) \times 10^{-6}, & [\text{CLEO}], \\ (62 \pm 18 \pm 8) \times 10^{-6}, & [\text{BaBar}], \end{cases} \quad (69)$$

$$\mathcal{B}(B \rightarrow K^0\eta') = (89_{-16}^{+18} \pm 9) \times 10^{-6}, \quad [\text{CLEO}]. \quad (70)$$

The measurements of CLEO, BaBar and Belle Collaborations are in good agreement with each other within errors. These decays are sensitive to the relevant form factors $F_0^{B \rightarrow \pi}, F_0^{B \rightarrow \eta}, F_0^{B \rightarrow \eta'}, \text{etc.}$, and to the value of N^{eff} .

As a Class-I decay channel, the $B^0 \rightarrow \pi^+\pi^-$ decay are dominated by the $b \rightarrow u$ tree diagram. The band between two dots lines in Fig.2 shows the CLEO measurement. Since the new physics corrections are very small in size, less than 3% within the considered parameter space, the four curves for the SM and 2HDM's are close together and can not be separated clearly. The theoretical predictions looks higher than the CLEO measurement, but they are consistent with BaBar measurement because of very large error of BaBar data. The CLEO data of $\mathcal{B}(B \rightarrow \pi^+\pi^-)$ prefer a small form factor $F_0^{B\pi} = 0.20 \pm 0.04$ as discussed in Ref. [48]. In fact the theoretical predictions for $\mathcal{B}(B \rightarrow \pi^+\pi^-)$ in the SM and 2HDM's are still consistent with the CLEO data at the 2σ level if we consider currently still large theoretical and experimental uncertainties.

In the SM, the four Class-IV decays $B \rightarrow K\pi$ are dominated by the $b \rightarrow sg$ gluonic penguin diagrams, with additional contributions from $b \rightarrow u$ tree and electroweak penguin diagrams. Measurements of $B \rightarrow K\pi$ decays are particularly important to measure the angle γ . In model III, the new physics enhancements to the branching ratios $\mathcal{B}(B \rightarrow K\pi)$ are significant, $\sim (50 - 60)\%$, and show a moderate dependence on the variations of other parameters, as illustrated in figures (3-6). In models I and II, however, the new physics corrections are always very small in size. For decays $B \rightarrow K^+\pi^-, K^0\pi^+$, the theoretical predictions in model III are higher than the CLEO data, they are in fact still consistent with the CLEO data at the 2σ level if we consider currently still large theoretical uncertainties.

Figures (3-6) show the mass and N^{eff} -dependence of the branching ratio for four $B \rightarrow K\pi$ decay modes in the SM and models I, II and III, using the input parameters as given in Eq.(7) and Appendix, and assuming $\theta = 0^0$, $\tan\beta = 2$, $k^2 = m_b^2/2$. For Figs.(3a-6a), we set $N^{eff} = 3$ and assume that $M_{H^+} = 100 - 300\text{GeV}$. For Figs.(3b-6b), we set $M_{H^+} = 200\text{GeV}$, and assume that $1/N^{eff} = 0 - 0.5$. In all four figures, the band between two dots lines shows the corresponding CLEO measurements with 2σ errors. For $B \rightarrow K^0\pi^0$ decay, the inclusion of new physics contribution will improve the agreement between the data and theoretical prediction, as illustrated in Fig.6. For other three $B \rightarrow K\pi$ decays, the theoretical predictions in the model III are still consistent with the data if the theoretical uncertainties are taken into account.

B. $B \rightarrow K\eta^{(\prime)}$ decays and new physics effects

For $B^+ \rightarrow K^+\eta$ and $B^0 \rightarrow K^0\eta$ decay modes, the new physics corrections are large (small) in model III (models I and II). The theoretical predictions in the SM and 2HDM's are consistent with the new CLEO upper limits.

For $B \rightarrow K\eta'$ decay modes, the situation is very interesting now. In 1997, CLEO firstly reported the unexpectedly large $B \rightarrow K\eta'$ rates [28], which is confirmed very recently by CLEO with the full CLEO II/II.V data sample of 19 million produced B mesons [23,29]. The $K\eta'$ signal is large, stable and has small errors ($\sim 14\%$). Those measured ratios are clearly much larger than the SM predictions as given in table (IV). In [48], Cheng and Yang considered various possible enhancements to $K\eta'$ decay modes in the framework of the SM⁶, but found that the net enhancement is not very large: $\mathcal{B}(B^\pm \rightarrow K^\pm\eta') = (40 - 50) \times 10^{-6}$, which is smaller than the CLEO data⁷. At present, it is indeed difficult to explain the observed large rate for $B \rightarrow K\eta'$ [23,29]. This fact strongly suggest the requirement for additional contributions unique to the η' meson in the framework of the SM, or from new physics beyond the SM.

In models I and II, the new physics contributions are too small (or negative) to provide the required enhancements. This feature remains unchanged within the considered range of $\tan\beta = 1 - 30$.

In model III, however, the new physics enhancements are significant, $\sim 60\%$, and have a moderate dependence on M_{H^\pm} and N^{eff} , as illustrated by the solid curves in Figs.(7-10) where only the central values of theoretical predictions in the model III are shown. If we take into account other theoretical uncertainties, the theoretical predictions for ratios $\mathcal{B}(B \rightarrow K\eta')$ in model III will become consistent with the CLEO data:

$$\mathcal{B}(B^+ \rightarrow K^+\eta') = \begin{cases} (69 - 92) \times 10^{-6}, & [\text{CLEO}] , \\ (20 - 52) \times 10^{-6}, & [\text{SM}] , \\ (34 - 74) \times 10^{-6}, & [\text{Model III}] , \end{cases} \quad (71)$$

$$\mathcal{B}(B^0 \rightarrow K^0\eta') = \begin{cases} (71 - 109) \times 10^{-6}, & [\text{CLEO}] , \\ (19 - 53) \times 10^{-6}, & [\text{SM}] , \\ (33 - 73) \times 10^{-6}, & [\text{Model III}] . \end{cases} \quad (72)$$

Here the major theoretical uncertainties induced by using different set of form factors and varying k^2, η and N^{eff} in the ranges of $\delta k^2 = \pm 2\text{GeV}^2$, $\delta\eta = \pm 0.08$ and $N^{eff} = 2 - \infty$ have been taken into account.

⁶As discussed in [5], $B \rightarrow K\eta'$ decay may get enhanced due to (i) a small m_s at the scale m_b , (ii) the sizable $SU(3)$ breaking, (iii) large $F_0^{B \rightarrow \eta'}$, (iv) the η' charm content, and (v) constructive interference in tree amplitudes. But these possible enhancements are partially washed out by the anomaly effect in the matrix element of pseudoscalar densities [15,57].

⁷Although this prediction is consistent with Belle measurement, one should note that the error of Belle measurement is still much larger than that of CLEO data. More statistics is clearly required for Belle to make a definite conclusion.

Figures (7,9) show the mass and N^{eff} dependence of $\mathcal{B}(B \rightarrow K\eta')$ in the SM and 2HDM's. The upper dots band shows the CLEO measurements with 2σ errors. The short-dashed, dot-dashed, long-dashed and solid curve refers to the theoretical predictions in the SM, models I, II and III, respectively. As shown explicitly in Figs.(8,10), in which the short-dashed, long-dashed and solid curve corresponds to the model III predictions for $N^{eff} = 2, 3, \infty$ respectively, the theoretical predictions become now consistent with the CLEO measurement due to the inclusion of new physics enhancement in model III.

VI. $B \rightarrow PV$ DECAYS

In tables (VII-IX) we present the branching ratios for the thirty seven $B \rightarrow PV$ decay modes involving $b \rightarrow d$ and $b \rightarrow s$ transitions in the SM and models I, II and III by using the BSW form factors and by employing generalized factorization approach. Theoretical predictions are made by using the same input parameters as those for the $B \rightarrow PP$ decays in last section.

For considered thirty seven $B \rightarrow PV$ decays, two general features are as follows:

- The theoretical predictions for those seven measured decay rates are consistent with CLEO data within 2σ errors. All other estimated branching ratios in the SM and 2HDM's as given in tables (VII-IX) are all consistent with the new CLEO upper limits.
- For most decay modes, the differences induced by using whether BSW or LQQSR form factors are small, $\sim 15\%$. We therefore use the BSW form factors only in the calculation of new physics effects.

There are so far seven measured branching ratios of $B \rightarrow PV$ decays. For the first three decay modes, $B \rightarrow \rho^\pm \rho^\mp, \rho^0 \pi^+, \omega \pi^+$, the new physics corrections are small in size, $< 5\%$, and have a weak dependence on M_{H^+} and N^{eff} , as shown in tables (VIII,IX). Consequently, the theoretical predictions in the SM and models I, II and III are agree well with CLEO measurements.

Since the appearance of very large $\mathcal{B}(B \rightarrow K\eta')$, the decay modes $B \rightarrow K^* \eta^{(\prime)}$ also draw more attentions now. Very recently, CLEO and Belle reported their first observation [22,23,27] of $B \rightarrow K^* \eta, K^{*+} \pi^-$ and $B \rightarrow K^+ \phi$ decays:

$$\mathcal{B}(B^+ \rightarrow K^{*+} \eta) = (26.4_{-8.2}^{+9.6} \pm 3.3) \times 10^{-6}, \quad (73)$$

$$\mathcal{B}(B^0 \rightarrow K^{*0} \eta) = (13.8_{-4.6}^{+5.5} \pm 1.6) \times 10^{-6}, \quad (74)$$

$$\mathcal{B}(B^0 \rightarrow K^{*+} \pi^-) = (22_{-6-5}^{+8+4}) \times 10^{-6}, \quad (75)$$

$$\mathcal{B}(B^+ \rightarrow K^+ \phi) = (17.2_{-5.4}^{+6.7} \pm 1.8) \times 10^{-6}, \quad (76)$$

while the theoretical predictions in the SM and model III are

$$\mathcal{B}(B^+ \rightarrow K^{*+} \eta) = \begin{cases} (2 - 4) \times 10^{-6}, & [\text{SM}] , \\ (2 - 5) \times 10^{-6}, & [\text{Model III}] , \end{cases} \quad (77)$$

$$\mathcal{B}(B^+ \rightarrow K^{*0} \eta) = \begin{cases} (2 - 5) \times 10^{-6}, & [\text{SM}] , \\ (3 - 6) \times 10^{-6}, & [\text{Model III}] , \end{cases} \quad (78)$$

$$\mathcal{B}(B^+ \rightarrow K^{*+}\pi^-) = \begin{cases} (7 - 16) \times 10^{-6}, & [\text{SM}] , \\ (10 - 22) \times 10^{-6}, & [\text{Model III}] , \end{cases} \quad (79)$$

$$\mathcal{B}(B^+ \rightarrow K^+\phi) = \begin{cases} (0.5 - 28) \times 10^{-6}, & [\text{SM}] , \\ (1 - 39) \times 10^{-6}, & [\text{Model III}] , \end{cases} \quad (80)$$

where the uncertainties induced by using the BSW or LQQSE form factors, and setting $k^2 = m_b^2/2 \pm 2\text{GeV}^2$, $\eta = 0.34 \pm 0.08$ and $N^{eff} = 2 - \infty$, have been taken into account. Although the central values of the theoretical predictions in the SM are much smaller than the corresponding central values of the CLEO measurements, the theoretical predictions are still consistent with the data within 2σ errors because current experimental error is still large. Further improvement of experimental measurements about the decay modes $B \rightarrow K^*\eta$, $K^{*+}\pi^-$ will tell us whether there is any discrepancy between the theory and experiments for these three decay modes. At present, any positive contributions to the above three branching ratios from new mechanisms in the SM or from new physics beyond the SM are clearly preferred by the CLEO data.

In models I and II, the new physics contributions are small in size: from -15% to 20% for most $B \rightarrow PV$ decay modes, and have weak dependence on M_{H^+} , $\tan\beta$ and N^{eff} , as shown in table (IX), and illustrated in Figs.(11-14) where the long-dashed line shows the theoretical predictions in the model II⁸. This feature remains unchanged within the considered range of $\tan\beta = 1 - 30$. When $\tan\beta$ becomes larger, the size of new physics corrections will become even smaller.

In model III, however, the new physics contributions are significant, from 30% to 110% , and have also weak dependence on M_{H^+} , θ and N^{eff} . These new physics enhancements are very helpful to improve the agreement between the theoretical predictions and the data, as shown in Eqs.(77-80) and illustrated in Figs.(11-14).

Figs.(11-14) show the mass and N^{eff} dependence of the branching ratios for $B \rightarrow K^{*+}\eta$, $K^{*0}\eta$, $K^{*+}\pi^-$ and $B \rightarrow K^+\phi$ decays. The dot-dashed line is the SM prediction, while the long-dashed and solid curve corresponds to the predictions in models II and III, respectively. The theoretical uncertainties are not shown in figures. The dots band corresponds to the CLEO data with 1σ error.

From Fig.(11), it can be seen that the CLEO measurement of the ratio $\mathcal{B}(B^+ \rightarrow K^{*+}\eta)$ is much larger than theoretical predictions in the SM and 2HDM's. More positive contributions to this decay mode are needed to improve the agreement between the data and theoretical prediction. For $B \rightarrow K^{*0}\eta$ decay, the inclusion of new physics contribution in the model III leads to a better agreement between data and theory if we take into account still large theoretical uncertainties. For $B \rightarrow K^{*+}\pi^-$ and $K^+\phi$ decays, the theoretical prediction becomes now consistent with the CLEO and Belle measurements within 1σ error due to the large new physics enhancement in the model III.

For two $B \rightarrow K^{*+}\eta'$, $K^{*0}\eta'$ decays, the new physics contributions in model III can also provide significant enhancements, from -77% to 200% , as shown in Table VIII. But the

⁸Because the lines for the SM and model I are too close to be separated clearly, we do not draw the line for the model I in all four figures for $B \rightarrow PV$ decays.

theoretical predictions for these two decay modes are N^{eff} -dependent and still far below the current CLEO upper limits.

VII. $B \rightarrow VV$ DECAYS

Using the formulae as given in Sec. IV, it is straightforward to calculate the branching ratios of nineteen $B_{u,d} \rightarrow VV$ decays. As an example, we show here the calculation of the branching ratio for the Class-V decay $B^- \rightarrow \rho^- \omega$ ($b \rightarrow d$ transition). We firstly find the explicit expressions of the helicity amplitude $H_\lambda = \langle \rho^-(\lambda) \omega(\lambda) | H_{eff} | B^- \rangle$, and then compare this amplitude with the standard form as defined in Eq.(54) to extract out the process dependent coefficients a, b and c

$$a = -\frac{1}{\sqrt{2}} \cdot \left[f_1 f_\omega M_\omega (M_B + M_\rho) A_1^{B \rightarrow \rho}(M_\omega^2) + f_2 f_\rho M_\rho (M_B + M_\omega) A_1^{B \rightarrow \omega}(M_\rho^2) \right], \quad (81)$$

$$b = f_1 \cdot \frac{\sqrt{2} f_\omega M_\omega^2 M_\rho}{M_B + M_\rho} A_2^{B \rightarrow \rho}(M_\omega^2) + f_2 \cdot \frac{\sqrt{2} f_\rho M_\rho^2 M_\omega}{M_B + M_\omega} A_2^{B \rightarrow \omega}(M_\rho^2), \quad (82)$$

$$c = f_1 \cdot \frac{\sqrt{2} f_\omega M_\omega^2 M_\rho}{M_B + M_\rho} V^{B \rightarrow \rho}(M_\omega^2) + f_2 \cdot \frac{\sqrt{2} f_\rho M_\rho^2 M_\omega}{M_B + M_\omega} V^{B \rightarrow \omega}(M_\rho^2), \quad (83)$$

with

$$f_1 = \frac{G_F}{\sqrt{2}} \left[V_{ub} V_{ud}^* a_2 - V_{tb} V_{td}^* \left(2a_3 + a_4 + 2a_5 + \frac{1}{2}a_7 + \frac{1}{2}a_9 - \frac{1}{2}a_{10} \right) \right], \quad (84)$$

$$f_2 = \frac{G_F}{\sqrt{2}} [V_{ub} V_{ud}^* a_1 - V_{tb} V_{td}^* (a_4 + a_{10})], \quad (85)$$

where the coefficients $a_{1,\dots,10}$ have been defined in Eq.(57), the form factors and other input parameters can be found in Appendix. With these coefficients a, b and c , the branching ratio $\mathcal{B}(B^- \rightarrow \rho^- \omega)$ can finally be written as

$$\mathcal{B}(B^- \rightarrow \rho^- \omega) = \tau_{B_u^-} \frac{|p|}{8\pi M_B^2} \left(|H_0|^2 + |H_{+1}|^2 + |H_{-1}|^2 \right) \quad (86)$$

with

$$|p| = \frac{1}{2M_B} \sqrt{[M_B^2 - (M_\rho + M_\omega)^2][M_B^2 - (M_\rho - M_\omega)^2]}, \quad (87)$$

$$H_{\pm 1} = a \pm c\sqrt{x^2 - 1}, \quad H_0 = -ax - b(x^2 - 1), \quad (88)$$

$$x = \frac{M_B^2 - M_\rho^2 - M_\omega^2}{2M_\rho M_\omega}, \quad (89)$$

In tables (X-XII) we present the branching ratios for the nineteen $B \rightarrow VV$ decay modes involving $b \rightarrow d$ and $b \rightarrow s$ transitions in the SM and models I, II and III. Theoretical predictions are made by using the same input parameters as those for the $B \rightarrow PP, PV$ decays in last two sections.

For $B \rightarrow VV$ decay modes, the differences induced by using whether BSW or LQQSR form factors are around ten percent in the SM and models I, II and III. We therefore show

the numerical results obtained by using the BSW form factors only for the cases of models I, II and III. For all nineteen $B \rightarrow VV$ decays under study, the theoretical predictions in the SM and 2HDM's are still under or far away from the current CLEO upper limits, as can be seen from tables (X-XII).

In models I and II, the new physics contributions to $B \rightarrow VV$ decays are small in size: from -15% to $\sim 10\%$ as shown in Table XII, and therefore will be masked by other large theoretical uncertainties. This feature remains unchanged within the considered range of $\tan\beta = 1 - 30$. When $\tan\beta$ becomes larger, the size of new physics corrections will become smaller.

In model III, however, the new physics contributions to different channels are varying greatly: from -11% to $\sim 110\%$, assuming $M_{H^+} = 200\text{GeV}$, $N^{eff} = 2 - \infty$ and $\theta = 0^0 - 30^0$. For decay modes $B \rightarrow K^{*0}\omega$, $K^{*+}\phi$, $K^{*0}\phi$, for example, the new physics enhancements are significant: $\sim (60 - 110)\%$. And hence the theoretical predictions in model III are close to or slightly surpass the current CLEO upper limits, as illustrated in Figs.(15-17) where the upper dots line shows the corresponding CLEO upper limits at $90\%C.L.$. These decay modes will be observed soon.

Figures (15-17) show the mass and N^{eff} dependence of the ratios $\mathcal{B}(B \rightarrow K^{*0}\omega)$ and $\mathcal{B}(B \rightarrow K^{*}\phi)$. The dot-dashed line is the SM predictions, while the long-dashed and solid curve corresponds to the predictions in models II and III, respectively. As Class-V decays, these three decays show strong N^{eff} dependence as illustrated in Figs.(15-17).

VIII. SUMMARY AND DISCUSSIONS

In this paper, we calculated the branching ratios of two-body charmless hadronic B meson decays $B_{u,d} \rightarrow PP, PV, VV$ in the SM and the general two-Higgs-doublet models by employing the NLO effective Hamiltonian with generalized factorization.

In Sec. II, with the help of previous works [38,42–44,35], we gave a brief review about the 2HDM's and studied corresponding experimental constraints on models I, II and III. In Sec. III, we evaluated analytically all new gluonic and electroweak charged-Higgs penguin diagrams and find the effective Wilson coefficients C_i^{eff} in the SM and models I, II and III. In Sec. IV, we presented the formulae needed to calculate the branching ratios $\mathcal{B}(B \rightarrow PP, PV, VV)$.

In sections V-VII, we calculated the branching ratios for seventy six $B \rightarrow PP, PV, VV$ decays in the SM and models I, II and III, presented the numerical results in tables (IV-XII) and displayed the M_{H^+} and N^{eff} -dependence for several phenomenologically interesting decay modes in Figs.(2-17).

From the numerical results, we find following general features about the new physics effects on exclusive charmless hadronic $B \rightarrow PP, PV, VV$ decays studied in this paper:

- 1 The SM predictions for the B meson decay rates presented in this paper are agree well with those appeared in Refs. [7,9].
- 2 The new physics effects due to new gluonic penguin diagrams strongly dominate over those from the γ - and Z^0 - penguin diagrams induced by exchanges of charged-Higgs bosons appeared in the models I, II and III.

- 3 For models I and II, the new physics contributions to the decay rates $\mathcal{B}(B \rightarrow h_1 h_2)$ are always small in size: from -15% to 20% for most decay modes. So small contributions will be masked by other still large theoretical uncertainties.
- 4 For model III, however, the new physics enhancements to penguin-dominated decay modes can be significant, $\sim (30 - 200)\%$, and therefore can be measured in high precision B experiments. In general, the new physics contributions in model III are large (small) for penguin- dominated (tree-dominated) B meson decay channels.
- 5 The uncertainties of the theoretical predictions for the branching ratios of $B \rightarrow h_1 h_2$ decays induced by varying k^2 , η , θ , $\tan \beta$, and M_{H^+} are varying from $\sim 10\%$ to $\sim 50\%$ within the range of $k^2 = m_b^2/2 \pm 2\text{GeV}^2$, $\eta = 0.34 \pm 0.08$, $\theta = 0^\circ - 30^\circ$, $\tan \beta = 1 - 30$, and $M_{H^+} = 200 \pm 100 \text{ GeV}$. The dependence of decay rates on whether using the BSW or LQSSR form factors are weak, $\sim 10\%$. The N^{eff} -dependence of branching ratios, however, are varying greatly for different decay modes.
- 6 For phenomenologically interesting $B \rightarrow K\eta'$ decay modes, the new physics corrections are significant in model III: $\sim (35 - 70)\%$, and have a moderate dependence on M_{H^+} and N^{eff} . The theoretical predictions for $\mathcal{B}(B \rightarrow K\eta')$ therefore turn to be consistent with the CLEO data in model III, as illustrated in Figs.(8,10). For other $B \rightarrow PP$ decays, the theoretical predictions are still consistent with the measurements if still large theoretical and experimental uncertainties are taken into account.
- 7 For penguin-dominated $B \rightarrow PV$ decays, the new physics contributions in model III are significant, from 30% to 60% , and have weak or moderate dependence on M_{H^+} , θ and N^{eff} , as illustrated in tables (VIII-VIII) and figures (11-14). The CLEO measurements of $\mathcal{B}(B \rightarrow K^{*+}\eta, K^{*0}\eta)$ are much larger than theoretical predictions in the SM and hence large new physics enhancements in model III are indeed helpful to lead to or improve the agreement between the data and theoretical predictions.
- 8 In model III, the new physics contributions to different $B \rightarrow VV$ decay modes are varying greatly: from -11% to $\sim 110\%$. For decay modes $B \rightarrow K^{*0}\omega, K^{*+}\phi, K^{*0}\phi$, for example, the new physics enhancements are significant: $\sim (60 - 110)\%$, and hence the theoretical predictions in model III are close to or slightly surpass the current CLEO upper limits. These decay modes will be observed soon.

ACKNOWLEDGMENTS

The authors are very grateful to D.S. Du, C.D. Lü, Y.D. Yang and M.Z. Yang for helpful discussions. C.S. Li and K.T. Chao acknowledge the support by the National Natural Science Foundation of China, the State Commission of Science and technology of China and the Doctoral Program Foundation of Institution of Higher Education. Z.J. Xiao acknowledges the support by the National Natural Science Foundation of China under the Grant No.19575015 and 10075013, and the Excellent Young Teachers Program of Ministry of Education, P.R.China.

APPENDIX A: INPUT PARAMETERS AND FORM FACTORS

In this appendix we present relevant input parameters. We use the same set of input parameters for the quark masses, decay constants, Wolfenstein parameters and form factors as Ref. [7].

- Input parameters of electroweak and strong coupling constant, gauge boson masses, B meson masses, light meson masses, \dots , are as follows (all masses in unit of GeV) [7,56]

$$\begin{aligned}
\alpha_{em} &= 1/128, \quad \alpha_s(M_Z) = 0.118, \quad \sin^2 \theta_W = 0.23, \quad G_F = 1.16639 \times 10^{-5} (GeV)^{-2}, \\
M_Z &= 91.187, \quad M_W = 80.41, \quad m_{B_d^0} = m_{B_u^\pm} = 5.279, \quad m_{\pi^\pm} = 0.140, \\
m_{\pi^0} &= 0.135, \quad m_\eta = 0.547, \quad m_{\eta'} = 0.958, \quad m_\rho = 0.770, \quad m_\omega = 0.782, \\
m_\phi &= 1.019, \quad m_{K^\pm} = 0.494, \quad m_{K^0} = 0.498, \quad m_{K^{*\pm}} = 0.892, \quad m_{K^{*0}} = 0.896, \\
\tau(B_u^\pm) &= 1.64 ps, \quad \tau(B_d^0) = 1.56 ps,
\end{aligned} \tag{A1}$$

- For the elements of CKM matrix, we use Wolfenstein parametrization, and fix the parameters A, λ, ρ to their central values, $A = 0.81$, $\lambda = 0.2205$, $\rho = 0.12$ and varying η in the range of $\eta = 0.34 \pm 0.08$.
- We first treat the internal quark masses in the loops in connection with the function $G(x_i, z)$ as constituent masses,

$$m_b = 4.88 GeV, \quad m_c = 1.5 GeV, \quad m_s = 0.5 GeV, \quad m_u = m_d = 0.2 GeV. \tag{A2}$$

Secondly, we will use the current quark masses for m_i ($i = u, d, s, c, b$) which appear through the equation of motion when working out the hadronic matrix elements. For $\mu = 2.5 GeV$, one finds [7]

$$m_b = 4.88 GeV, \quad m_c = 1.5 GeV, \quad m_s = 0.122 GeV, \quad m_d = 7.6 MeV, \quad m_u = 4.2 MeV. \tag{A3}$$

For the mass of heavy top quark we also use $m_t = \overline{m}_t(m_t) = 168 GeV$.

- For the decay constants of light mesons, the following values will be used in the numerical calculations (in the units of MeV):

$$\begin{aligned}
f_\pi &= 133, \quad f_K = 158, \quad f_{K^*} = 214, \quad f_\rho = 210, \quad f_\omega = 195, \quad f_\phi = 233, \\
f_\eta^u &= f_\eta^d = 78, \quad f_{\eta'}^u = f_{\eta'}^d = 68, \quad f_\eta^c = -0.9, \quad f_{\eta'}^c = -0.23, \\
f_\eta^s &= -113, \quad f_{\eta'}^s = 141.
\end{aligned} \tag{A4}$$

where $f_{\eta^{(\prime)}}$ and $f_{\eta^{(\prime)}}$ have been defined in the two-angle-mixing formalism with $\theta_0 = -9.1^\circ$ and $\theta_8 = -22.2^\circ$ [58] For more details about the mixings between η and η' , one can see [58,15].

- The form factors at the zero momentum transfer in the Baner, Stech and Wirbel (BSW) [13] model have been collected in Table 2 of Ref. [7]. For the convenience of the reader we list them here:

$$\begin{aligned}
F_0^{B \rightarrow \pi}(0) &= 0.33, \quad F_0^{B \rightarrow K}(0) = 0.38, \quad F_0^{B \rightarrow \eta}(0) = 0.145, \quad F_0^{B \rightarrow \eta'}(0) = 0.135, \\
A_{0,1,2}^{B \rightarrow \rho}(0) &= A_{0,1,2}^{B \rightarrow \omega}(0) = 0.28, \quad A_0^{B \rightarrow K^*}(0) = 0.32, \quad A_{1,2}^{B \rightarrow K^*}(0) = 0.33, \\
V^{B \rightarrow \rho}(0) &= V^{B \rightarrow \omega}(0) = 0.33, \quad V^{B \rightarrow K^*}(0) = 0.37,
\end{aligned} \tag{A5}$$

- In the LQQSR approach, the form factors at zero momentum transfer being used in our numerical calculations are,

$$\begin{aligned}
F_0^{B \rightarrow \pi}(0) &= 0.36, \quad F_0^{B \rightarrow K}(0) = 0.41, \quad F_0^{B \rightarrow \eta}(0) = 0.16, \quad F_0^{B \rightarrow \eta'}(0) = 0.145, \\
\{A_0, A_1, A_2, V\}(B \rightarrow \rho) &= \{0.30, 0.27, 0.26, 0.35\}, \\
\{A_0, A_1, A_2, V\}(B \rightarrow K^*) &= \{0.39, 0.35, 0.34, 0.48\}, \\
\{A_0, A_1, A_2, V\}(B \rightarrow \omega) &= \{0.30, 0.27, 0.26, 0.35\}.
\end{aligned} \tag{A6}$$

- The form factors $F_{0,1}(k^2)$, $A_{0,1,2}(k^2)$ and $V(k^2)$ were defined in Ref. [13] as

$$\begin{aligned}
F_0(k^2) &= \frac{F_0(0)}{1 - k^2/m^2(0^+)}, \quad F_1(k^2) = \frac{F_1(0)}{1 - k^2/m^2(1^-)}, \\
A_0(k^2) &= \frac{A_0(0)}{1 - k^2/m^2(0^-)}, \quad A_1(k^2) = \frac{A_1(0)}{1 - k^2/m^2(1^+)}, \\
A_2(k^2) &= \frac{A_2(0)}{1 - k^2/m^2(1^+)}, \quad V(k^2) = \frac{V(0)}{1 - k^2/m^2(1^-)}.
\end{aligned} \tag{A7}$$

- The pole masses being used to evaluate the k^2 -dependence of form factors are, and

$$\{m(0^-), m(1^-), m(1^+), m(0^+)\} = \{5.2789, 5.3248, 5.37, 5.73\}, \tag{A8}$$

for $\bar{u}b$ and $\bar{d}b$ currents. And

$$\{m(0^-), m(1^-), m(1^+), m(0^+)\} = \{5.3693, 5.41, 5.82, 5.89\}, \tag{A9}$$

for $\bar{s}b$ currents.

REFERENCES

- [1] P.F. Harrison and H.R. Quinn, Editors, *The BaBar Physics Book*, SLAC-R-504, 1998.
- [2] M.T. Cheng *et al.*, Belle collaboration, KEK-Report 94-2; F. Takasaki, hep-ex/9912004.
- [3] R. Fleischer and J. Matias, Phys.Rev.**D61**, 074004(2000).
- [4] A.J. Buras and R.Fleischer, Talk presented at ICHEP 2000, Osaka, Japan, 27 July - 2 August 2000, hep-ph/0008298; P.Ball, Talk given at IVth Rencontres de Vietnam, Hanoi, July 2000, hep-ph/0010024; C.D. Lü, Talk given at BCONF 99, Taipei, Taiwan, 3-7 Dec. 1999, hep-ph/0001321;
- [5] H.-Y. Cheng, Presented at ICHEP 2000, Osaka, Japan, 27 July - 2 August 2000, hep-ph/0008285.
- [6] D. Du and L. Guo, Z.Phys. **C75**, 9(1997); D. Du and L. Guo, J. Phys. **G23**, 525(1997).
- [7] A. Ali, G. Kramer and C.D. Lü, Phys.Rev. **D58**, 094009(1998).
- [8] A. Ali, G. Kramer and Cai-Dian Lü, Phys.Rev. **D59**, 014005(1999).
- [9] Y.H. Chen, H.Y. Cheng, B. Tseng and K.C. Yang, Phys.Rev. **D60**, 094014(1999).
- [10] H. Simma and D. Wyler, Phys.Lett. **B272**, 395 (1991); G. Kramer, W.F. Palmer and H. Simma, Nucl.Phys. **B428**, 77(1994); Z.Phys. **C66**, 429(1995); R. Fleischer, Phys.Lett. **B321**, 259(1994); Z.Phys. **C62**, 81(1994); G. Kramer and W.F. Palmer, Phys.Rev. **D52**, 6411(1995); N.G. Deshpande and X.G. He, Phys.Lett. **B336**, 471(1994); G. Kramer, W.F. Palmer and Y.L. Wu, Commun.Theor.Phys. **27**, 457(1997);
- [11] G. Buchalla, A.J. Buras and M.E. Lautenbacher, Rev.Mod.Phys. **68**, 1125(1996).
- [12] A.J. Buras and R. Fleischer, in *Heavy Flavor II*, ed. A.J.Buras and M.Lindner (World Scientific, Singapore, 1998), page-65; A.J. Buras, in *Probing the Standard model of Particle Interactions*, ed. F.David and R.Gupta, 1998 Elsevier Science B.V., hep-ph/9806471.
- [13] M. Bauer and B. Stech, Phys.Lett. **B152**, 380 (1985);
M. Bauer, B. Stech and M. Wirbel, Z. Phys. **C29**, 637 (1985); *ibid*, **C34**, 103 (1987).
- [14] H.-Y. Cheng, Phys.Lett. **B335**, 428(1994); **B395**, 345(1997); H.-Y. Cheng and B.Tseng, Phy.Rev. **D58**, 094005 (1998).
- [15] A. Ali, C. Greub, Phys.Rev **D57**, 2996 (1998); A. Ali, J. Chay, C. Greub and P. Ko, Phys.Lett. **B424**, 161(1998).
- [16] K.G. Wilson, Phys.Rev. **179**, 1499(1969).
- [17] A.J. Buras, L. Silvestrini, Nucl.Phys. **B548**, 293(1999).
- [18] H.-Y. Cheng, Hsiang-nan Li and K.C. Yang, Phys.Rev. **D60**, 094005(1999).
- [19] M. Beneke, G. Buchalla, M. Neubert and C.T. Sachrajda, Phys.rev.Lett. **83**, 1914 (1999); See preprint hep-ph/0007256 for recent progress.
- [20] Y.-Y. Keum, H.-n. Li and A. Sanda, hep-ph/0004173.
- [21] D.S. Du, D.S. Yang and G.H. Zhu, Phys.Lett. **B488**, 46(2000); T. Muta, A. Sugamoto, M.Z. Yang and Y.D. Yang, hep-ph/0006022.
- [22] Y. Gao and F. Würthwein, CLEO Collaboration, hep-ex/9904008, DPF99 Proceedings. M. Bishai *et al.*, CLEO Collaboration, CLEO CONF 99-13, hep-ex/9908018; S.J. Richichi *et al.*, CLEO Collaboration, CLEO CONF 99-12, hep-ex/9908019; T.E. Coan *et al.*, CLEO Collaboration, CLEO CONF 99-16, hep-ex/9908029; Y. Kwon *et al.*, CLEO Collaboration, CLEO CONF 99-14, hep-ph/9908039.
- [23] S.J. Richichi *et al.*, CLEO Collaboration, Phys.Rev.Lett. **85**, 520(2000).
- [24] D. Cronin-Hennessy *et al.*, CLEO Collaboration, Phys.Rev.Lett. **85**, 515(2000); C.P. Jessop *et al.*, CLEO Collaboration, CLEO 99-19, hep-ex/0006008.

- [25] D. Jaffe, Talk Presented at BNL Particle Physics Seminar, 20 April, 2000, CLEO Talk 00-10; D. Urner, Talk presented at DPF 2000, 12 August, 2000, CLEO Talk 00-33.
- [26] J. Olson, (BaBar Collaboration), Talk presented at DPF 2000, 12 August, 2000, BaBar Talk 00/27; F. Ferroni, (BaBar Collaboration), Talk presented at DPF 2000, 12 August, 2000, BaBar Talk 00/12. B.Aubert *et al.*, BaBar Collab., hep-ex/0008057.
- [27] A.Abashian *et al.*, Belle Collaboration, Contributed papers for ICHEP 2000, Belle-Conf-0005, Belle-Conf-0006, Belle-Conf-0007.
- [28] B.H. Behrens *et al.*, CLEO Collaboration, Phys.Rev.Lett. **80**, 3710(1998); T.E. Browder *et al.*, CLEO Collaboration, Phys.Rev.Lett. **81**, 1786 (1998).
- [29] A. Gritsan, Talk presented at UCSB, UCSD, LBNL, SLAC, CU-Boulder, March-May 2000, CLEO TALK 00-20.
- [30] Chao-Qiang Geng, P. Turcotte and W.S. Hou, Phys.Lett. **B339**, 317(1994).
- [31] A.L. Kagan, Phys.Rev. **D51**, 6196 (1995); A.L. Kagan, hep-ph/9806266, Proceedings of the Seventh International Symposium on Heavy Flavor Physics, Santa Barbara CA, July 1997.
- [32] W.S. Hou and B. Tseng, Phys.Rev.Lett. **80**, 434 (1998); A.L. Kagan and A.A. Petrov, hep-ph/9707354.
- [33] G.R. Lu, Z.J. Xiao, H.K. Guo and L.X. Lü, J. Phys. **G25**, L85 (1999).
- [34] Z.J. Xiao, C.S. Li and K.T. Chao, Phys.Lett. **B473**, 148(2000).
- [35] Z.J. Xiao, C.S. Li and K.T. Chao, Phys.Rev. **D62**, 094008(2000).
- [36] A. Lenz, U. Nierste and G. Ostermaier, Phys.Rev. **D56**, 7228 (1997).
- [37] S. Glashow and S. Weinberg, Phys.Rev. **bf D15**, 1958(1977).
- [38] D.Atwood, L.Reina and A.Soni, Phys.Rev. **bf D55**, 3156 (1997).
- [39] T.P.Cheng and M.Sher, Phys.Rev. **D35**, 3484(1987); M.Sher and Y.Yuan, Phys.Rev. **D44**, 1461(1991); W.S.Hou, Phys.Lett. **B296**, 179(1992); A. Antaramian, L.J. Hall and A. Rasin, Phys. Rev. Lett. **69**, 1871 (1992); L.J.Hall and S.Winberg, Phys.Rev. **D48**, R979 (1993); D.Chang, W.S.Hou and W.Y.Keung, Phys.Rev. **D48**, 217 (1993); Y.L.Wu and L. Wolfenstein, Phys.Rev.Lett. **73**, 1762 (1994); D. Atwood, L.Reina and A.Soni, Phys.Rev. Lett. **75**, 3800 (1995).
- [40] M.Kabayashi and T.Maskawa, Prog. Theor. Phys. **49**, 652 (1973).
- [41] F.M.Borzumati and C. Greub, Phys.Rev. **D58**, 074004 (1998), *ibid*, Phys.Rev. **D59**, 057501 (1999) (Addendum).
- [42] D. Atwood, L. Reina and A. Soni, Phys.Rev. **D54**, 3296 (1996).
- [43] T.M. Aliev and E.O. Iltan, J.Phys.**G25**, 989 (1999).
- [44] D. B. Chao, K. Cheung and W.Y. Keung, Phys.Rev. **D59**, 115006 (1999).
- [45] E.Gross, "Searches for New Physics", To be published in the proceedings of EPS-HEP 99, Tampere, Finland, 15-21 July 1999.
- [46] T.Inami and C.S. Lim, Prog.Theor.Phys. **65**, 297 (1981); *ibid*, 65, 1772E (1981).
- [47] R. Fleischer, Z.Phys.**C58**, 483(1993).
- [48] H.-Y. Cheng and K.C. Yang, Phys.Rev. **D62**, 054029(2000).
- [49] S.A. Abel, W.N. Cottingham and I.B. Whittingham, Phys.Rev. **D58**, 073006(1998).
- [50] M. Bander, G. Silverman and A. Soni, Phys.Rev.Lett. **43**, 242(1979);
- [51] J.M. Gérard and W.S. Hou, Phys.Rev. **D43**, 2909(1991).
- [52] For more details about LQQSR form factors, one can see: J.M. Flynn and C.T. Sachrajda, preprint SHEP-97-20, hep-lat/9710057, and reference therein.

- [53] R.P. Feynman in *Symmetries in Particle Physics*, ed. A. Zichichi (Acad. Press, 1965) 167; O. Haan and B. Stech, Nucl.Phys. **B22**, 448 (1970).
- [54] J. Ellis, M.K. Gaillard and D.V. Nanopoulos, Nucl.Phys. **B100**, 313 (1975); D. Fakirov and B. Stech, Nucl.Phys. **B133**, 315 (1978); A. Ali, J. Körner, G. Kramer and J. Willrodt, Z. Phys. **C1**, 203(1979).
- [55] J. Bijnens and F. Hoogeveen, Phys.Lett. **B283**, 434(1992).
- [56] Particle Data Group, C. Caso *et al.*, Eur. Phys. J. **C3**,1(1998).
- [57] A.L. Kagan and A.A. Petrov, hep-ph/9707354.
- [58] T. Feldmann and P. Kroll, Eur.Phys.J. **C5**, 327 (1998).

TABLES

TABLE I. Wilson coefficients $C_i(\mu)$ and $C_g^{eff}(\mu)$ in the SM and models I, II and III at the scale $\mu = 2.5$ GeV, with $M_{H^+} = 200$ GeV, $\tan\beta = 2$ and $\theta = 0^0, 30^0$.

	SM	Model I	Model II	Model III: $\theta = 0^0$	Model III: $\theta = 30^0$
C_1	1.1245	1.1245	1.1245	1.1245	1.1245
C_2	-0.2662	-0.2662	-0.2662	-0.2662	-0.2662
C_3	0.0186	0.0187	0.0187	0.0186	0.0186
C_4	-0.0458	-0.0458	-0.0458	-0.0458	-0.0458
C_5	0.0113	0.0113	0.0113	0.0113	0.0113
C_6	-0.0587	-0.0585	-0.0585	-0.0587	-0.0587
C_7	0.0006	0.0006	0.0006	0.0006	0.0006
C_8	0.0007	0.0007	0.0007	0.0007	0.0007
C_9	-0.0095	-0.0099	-0.0099	-0.0096	-0.0096
C_{10}	0.0026	0.0027	0.0027	0.0026	0.0026
C_g^{eff}	-0.1527	-0.1321	-0.2487	0.3364	$0.2708 + 0.2448i$

TABLE II. Numerical values of a_i for the transitions $b \rightarrow d$ [$\bar{b} \rightarrow \bar{d}$]. The first, second and third entries for a_3, \dots, a_{10} refer to the values of a_i in the SM and models II and III, respectively. All entries for a_3, \dots, a_{10} should be multiplied with 10^{-4} .

	$N^{eff} = 2$	$N^{eff} = 3$	$N^{eff} = \infty$
a_1	0.995 [0.995]	1.061 [1.061]	1.192 [1.192]
a_2	0.201 [0.201]	0.026 [0.026]	-0.395 [-0.395]
a_3	$-16 - 7i$ [$-25 - 23i$]	77 [77]	$261 + 13i$ [$280 + 47i$]
	$-10 - 7i$ [$-19 - 23i$]	77 [77]	$252 + 13i$ [$271 + 47i$]
	$-40 - 7i$ [$-49 - 23i$]	77 [77]	$310 + 13i$ [$329 + 47i$]
a_4	$-423 - 33i$ [$-470 - 117i$]	$-467 - 35i$ [$-517 - 125i$]	$-554 - 39i$ [$-610 - 141i$]
	$-398 - 33i$ [$-445 - 117i$]	$-440 - 35i$ [$-490 - 125i$]	$-524 - 39i$ [$-581 - 141i$]
	$-546 - 33i$ [$-592 - 117i$]	$-597 - 35i$ [$-648 - 125i$]	$-701 - 39i$ [$-757 - 141i$]
a_5	$-193 - 7i$ [$-202 - 23i$]	-71 [-71]	$171 + 13i$ [$190 + 47i$]
	$-187 - 7i$ [$-196 - 24i$]	-71 [-71]	$161 + 13i$ [$180 + 47i$]
	$-217 - 7i$ [$-226 - 23i$]	-71 [-71]	$220 + 13i$ [$239 + 47i$]
a_6	$-642 - 33i$ [$-689 - 117i$]	$-671 - 35i$ [$-721 - 125i$]	$-728 - 39i$ [$-784 - 141i$]
	$-616 - 33i$ [$-663 - 117i$]	$-642 - 35i$ [$-693 - 125i$]	$-696 - 39i$ [$-752 - 141i$]
	$-764 - 33i$ [$-811 - 117i$]	$-801 - 35i$ [$-851 - 125i$]	$-874 - 39i$ [$-931 - 141i$]
a_7	$8.1 - 0.9i$ [$7.7 - 1.7i$]	$6.8 - 0.9i$ [$6.4 - 1.7i$]	$4.3 - 0.9i$ [$3.9 - 1.7i$]
	$9.3 - 0.9i$ [$8.9 - 1.7i$]	$8.0 - 0.9i$ [$7.5 - 1.7i$]	$5.3 - 0.9i$ [$4.9 - 1.7i$]
	$8.3 - 0.9i$ [$7.9 - 1.7i$]	$7.0 - 0.9i$ [$6.6 - 1.7i$]	$4.5 - 0.9i$ [$4.1 - 1.7i$]
a_8	$9.7 - 0.5i$ [$9.5 - 0.8i$]	$9.0 - 0.3i$ [$8.8 - 0.6i$]	7.5 [7.5]
	$11 - 0.5i$ [$11 - 0.8i$]	$9.9 - 0.3i$ [$9.7 - 0.6i$]	8.1 [8.1]
	$9.9 - 0.5i$ [$9.7 - 0.8i$]	$9.1 - 0.3i$ [$9.0 - 0.6i$]	7.6 [7.6]
a_9	$-84 - 0.9i$ [$-84 - 1.7i$]	$-90 - 0.9i$ [$-90 - 1.7i$]	$-102 - 0.9i$ [$-102 - 1.7i$]
	$-87 - 0.9i$ [$-87 - 1.7i$]	$-93 - 0.9i$ [$-94 - 1.7i$]	$-106 - 0.9i$ [$-106 - 1.7i$]
	$-84 - 0.9i$ [$-85 - 1.7i$]	$-90 - 0.9i$ [$-91 - 1.7i$]	$-103 - 0.9i$ [$-103 - 1.7i$]
a_{10}	$-14 - 0.5i$ [$-15 - 0.8i$]	$2.6 - 0.3i$ [$2.5 - 0.6i$]	37 [37]
	$-15 - 0.5i$ [$-15 - 0.8i$]	$2.8 - 0.3i$ [$2.7 - 0.6i$]	38 [38]
	$-15 - 0.5i$ [$-15 - 0.8i$]	$2.7 - 0.3i$ [$2.5 - 0.6i$]	37 [37]

TABLE III. Same as Table II but for $b \rightarrow s$ [$\bar{b} \rightarrow \bar{s}$] transitions.

	$N^{eff} = 2$	$N^{eff} = 3$	$N^{eff} = \infty$
a_1	0.995 [0.995]	1.061 [1.061]	1.192 [1.192]
a_2	0.201 [0.201]	0.026 [0.026]	-0.395 [-0.395]
a_3	$-21 - 14i$ [$-19 - 14i$]	77 [77]	$272 + 29i$ [$269 + 29i$]
	$-15 - 14i$ [$-14 - 14i$]	77 [77]	$262 + 29i$ [$260 + 29i$]
	$-45 - 14i$ [$-44 - 14i$]	77 [77]	$320 + 29i$ [$318 + 29i$]
a_4	$-449 - 72i$ [$-442 - 72i$]	$-494 - 77i$ [$-487 - 77i$]	$-585 - 86i$ [$-576 - 86i$]
	$-424 - 72i$ [$-417 - 72i$]	$-468 - 77i$ [$-460 - 77i$]	$-555 - 87i$ [$-547 - 87i$]
	$-571 - 72i$ [$-564 - 72i$]	$-625 - 77i$ [$-617 - 77i$]	$-732 - 86i$ [$-723 - 86i$]
a_5	$-198 - 14i$ [$-196 - 14i$]	-71 [-71]	$181 + 29i$ [$179 + 29i$]
	$-192 - 14i$ [$-191 - 14i$]	-71 [-71]	$172 + 29i$ [$169 + 29i$]
	$-222 - 14i$ [$-221 - 14i$]	-71 [-71]	$230 + 29i$ [$228 + 29i$]
a_6	$-667 - 72i$ [$-660 - 72i$]	$-698 - 77i$ [$-691 - 77i$]	$-758 - 86i$ [$-750 - 86i$]
	$-641 - 72i$ [$-635 - 72i$]	$-670 - 77i$ [$-663 - 77i$]	$-727 - 87i$ [$-719 - 87i$]
	$-790 - 72i$ [$-783 - 72i$]	$-828 - 77i$ [$-821 - 77i$]	$-905 - 86i$ [$-897 - 87i$]
a_7	$7.9 - 1.3i$ [$7.9 - 1.3i$]	$6.6 - 1.3i$ [$6.7 - 1.3i$]	$4.1 - 1.3i$ [$4.2 - 1.3i$]
	$9.1 - 1.3i$ [$9.2 - 1.3i$]	$7.7 - 1.3i$ [$7.8 - 1.3i$]	$5.0 - 1.3i$ [$5.1 - 1.3i$]
	$8.1 - 1.3i$ [$8.2 - 1.3i$]	$6.8 - 1.3i$ [$6.9 - 1.3i$]	$4.3 - 1.3i$ [$4.3 - 1.3i$]
a_8	$9.6 - 0.6i$ [$9.6 - 0.6i$]	$8.9 - 0.4i$ [$8.9 - 0.4i$]	7.5 [7.5]
	$10.6 - 0.6i$ [$10.6 - 0.6i$]	$9.8 - 0.4i$ [$9.8 - 0.4i$]	8.1 [8.1]
	$9.8 - 0.6i$ [$9.8 - 0.6i$]	$9.1 - 0.4i$ [$9.1 - 0.4i$]	7.6 [7.6]
a_9	$-84 - 1.3i$ [$-84 - 1.3i$]	$-90 - 1.3i$ [$-90 - 1.3i$]	$-102 - 1.3i$ [$-102 - 1.3i$]
	$-87 - 1.3i$ [$-87 - 1.3i$]	$-94 - 1.3i$ [$-94 - 1.3i$]	$-106 - 1.3i$ [$-106 - 1.3i$]
	$-85 - 1.3i$ [$-84 - 1.3i$]	$-91 - 1.3i$ [$-91 - 1.3i$]	$-103 - 1.3i$ [$-103 - 1.3i$]
a_{10}	$-15 - 0.6i$ [$-14 - 0.6i$]	$2.6 - 0.4i$ [$2.6 - 0.4i$]	37 [37]
	$-15 - 0.6i$ [$-15 - 0.6i$]	$2.8 - 0.4i$ [$2.8 - 0.4i$]	38 [38]
	$-15 - 0.6i$ [$-15 - 0.6i$]	$2.6 - 0.4i$ [$2.6 - 0.4i$]	37 [37]

TABLE IV. $\mathcal{B}(B \rightarrow PP)$ (in units of 10^{-6}) in the SM using the BSW [LQSSR] form factors, with $k^2 = m_b^2/2$ and $N^{eff} = 2, 3, \infty$. The last column shows the CLEO measurements and upper limits at 90%*C.L.* [22-25].

Channel	Class	$N^{eff} = 2$	$N^{eff} = 3$	$N^{eff} = \infty$	Data
$B^0 \rightarrow \pi^+\pi^-$	I	9.10 [10.8]	10.3 [12.3]	13.0 [15.5]	$4.3_{-1.5}^{+1.6} \pm 0.5$
$B^0 \rightarrow \pi^0\pi^0$	II	0.28 [0.33]	0.15 [0.18]	0.92 [1.09]	< 9.3
$B^+ \rightarrow \pi^+\pi^0$	III	6.41 [7.62]	5.06 [6.02]	2.85 [3.39]	< 12.7
$B^0 \rightarrow \eta\eta$	II	0.14 [0.17]	0.10 [0.13]	0.29 [0.36]	< 18
$B^0 \rightarrow \eta\eta'$	II	0.14 [0.17]	0.08 [0.09]	0.38 [0.45]	< 27
$B^0 \rightarrow \eta'\eta'$	II	0.04 [0.05]	0.01 [0.01]	0.13 [0.15]	< 47
$B^+ \rightarrow \pi^+\eta$	III	3.51 [4.25]	2.78 [3.37]	1.75 [2.13]	< 5.7
$B^+ \rightarrow \pi^+\eta'$	III	2.49 [2.90]	1.88 [2.17]	1.02 [1.17]	< 12
$B^0 \rightarrow \pi^0\eta$	V	0.26 [0.31]	0.29 [0.35]	0.39 [0.47]	< 2.9
$B^0 \rightarrow \pi^0\eta'$	V	0.06 [0.07]	0.08 [0.09]	0.14 [0.17]	< 5.7
$B^+ \rightarrow K^+\pi^0$	IV	12.0 [14.3]	13.5 [16.0]	16.7 [19.8]	$11.6_{-2.7}^{+3.0+1.4} \pm 1.2$
$B^0 \rightarrow K^+\pi^-$	IV	17.8 [21.2]	19.8 [23.5]	24.0 [28.5]	$17.2_{-2.4}^{+2.5} \pm 1.2$
$B^+ \rightarrow K^0\pi^+$	IV	19.9 [23.7]	23.2 [27.7]	30.6 [36.4]	$18.2_{-4.0}^{+4.6} \pm 1.6$
$B^0 \rightarrow K^0\pi^0$	IV	7.27 [8.68]	8.31 [9.92]	10.7 [12.7]	$14.6_{-5.1}^{+5.9+2.4} \pm 3.3$
$B^+ \rightarrow K^+\eta$	IV	3.91 [4.37]	4.56 [5.10]	6.07 [6.80]	< 6.9
$B^+ \rightarrow K^+\eta'$	IV	22.6 [26.2]	28.5 [33.1]	42.4 [49.2]	$80_{-9}^{+10} \pm 7$
$B^0 \rightarrow K^0\eta$	IV	3.22 [3.57]	3.63 [4.02]	4.58 [5.07]	< 9.3
$B^0 \rightarrow K^0\eta'$	IV	21.9 [25.5]	28.2 [32.7]	43.0 [49.9]	$89_{-16}^{+18} \pm 9$
$B^+ \rightarrow K^+\bar{K}^0$	IV	1.16 [1.35]	1.35 [1.58]	1.78 [2.07]	< 5.1
$B^0 \rightarrow K^0\bar{K}^0$	IV	1.10 [1.28]	1.28 [1.49]	1.68 [1.96]	< 17

TABLE V. $\mathcal{B}(B \rightarrow PP)$ (in units of 10^{-6}) in model III using the BSW form factors, with $k^2 = m_b^2/2$, $N^{eff} = 2, 3, \infty$, $M_{H^+} = 200\text{GeV}$ and $\theta = 0^0, 30^0$, respectively.

Channel	$\theta = 0^0$			$\delta\mathcal{B} [\%]$			$\theta = 30^0$			$\delta\mathcal{B} [\%]$		
	2	3	∞	2	3	∞	2	3	∞	2	3	∞
$B^0 \rightarrow \pi^+\pi^-$	9.33	10.6	13.3	2.5	2.5	2.4	8.83	10.0	12.6	-3.0	-3.1	-3.1
$B^0 \rightarrow \pi^0\pi^0$	0.36	0.25	1.03	30	61	13	0.39	0.23	0.92	40	52	-0.5
$B^+ \rightarrow \pi^+\pi^0$	6.41	5.06	2.85	0.0	0.0	0.0	6.41	5.06	2.85	0.0	0.0	0.0
$B^0 \rightarrow \eta\eta$	0.18	0.15	0.36	29	47	21	0.16	0.14	0.38	15	39	29
$B^0 \rightarrow \eta\eta'$	0.19	0.13	0.46	29	68	20	0.16	0.12	0.506	9.6	57	30
$B^0 \rightarrow \eta'\eta'$	0.05	0.02	0.15	20	127	17	0.04	0.02	0.16	-5.4	103	30
$B^+ \rightarrow \pi^+\eta$	3.82	3.13	2.20	8.7	13	26	3.48	2.81	1.95	-1.1	1.2	12
$B^+ \rightarrow \pi^+\eta'$	2.63	2.05	1.27	5.4	9.0	24	2.37	1.81	1.09	-4.8	-3.5	6.5
$B^0 \rightarrow \pi^0\eta$	0.39	0.44	0.59	50	51	49	0.36	0.42	0.57	39	43	46
$B^0 \rightarrow \pi^0\eta'$	0.11	0.14	0.25	92	91	72	0.10	0.13	0.25	65	76	70
$B^+ \rightarrow K^+\pi^0$	17.4	19.6	24.4	45	45	46	17.2	19.3	23.8	43	43	43
$B^0 \rightarrow K^+\pi^-$	26.8	29.9	36.5	51	51	53	26.5	29.5	36.1	49	49	51
$B^+ \rightarrow K^0\pi^+$	29.8	34.6	45.3	50	49	48	28.6	33.3	43.5	44	43	42
$B^0 \rightarrow K^0\pi^0$	11.4	13.0	16.7	57	57	56	10.8	12.5	16.1	49	50	51
$B^+ \rightarrow K^+\eta$	5.69	6.63	8.78	45	45	45	5.30	6.22	8.34	36	36	37
$B^+ \rightarrow K^+\eta'$	38.0	46.9	67.5	68	65	59	36.8	45.2	64.9	63	59	53
$B^0 \rightarrow K^0\eta$	4.86	5.50	6.93	51	51	51	4.63	5.27	6.73	44	45	47
$B^0 \rightarrow K^0\eta'$	36.7	45.9	67.3	67	63	57	35.1	43.8	64.2	60	56	49
$B^+ \rightarrow K^+\bar{K}^0$	1.73	2.01	2.62	49	48	47	1.64	1.91	2.49	41	41	40
$B^0 \rightarrow K^0\bar{K}^0$	1.64	1.90	2.48	49	48	47	1.55	1.80	2.36	41	41	40

TABLE VI. $\mathcal{B}(B \rightarrow PP)$ (in units of 10^{-6}) in models I and II using the BSW form factors, with $k^2 = m_b^2/2$, $N^{eff} = 2, 3, \infty$, $\tan \beta = 2$ and $M_{H^+} = 200\text{GeV}$.

Channel	model I			$\delta\mathcal{B} [\%]$			model II			$\delta\mathcal{B} [\%]$		
	2	3	∞	2	3	∞	2	3	∞	2	3	∞
$B^0 \rightarrow \pi^+\pi^-$	9.11	10.3	13.0	0.1	0.1	0.1	9.1	10.3	13.0	-0.5	-0.4	-0.4
$B^0 \rightarrow \pi^0\pi^0$	0.28	0.15	0.92	-0.1	-0.1	0.1	0.3	0.1	0.9	-6.2	-12.6	-2.5
$B^+ \rightarrow \pi^+\pi^0$	6.41	5.06	2.85	0.0	0.0	0.0	6.4	5.1	2.9	0.0	0.0	0.0
$B^0 \rightarrow \eta\eta$	0.14	0.11	0.30	1.5	2.4	1.1	0.1	0.1	0.3	-4.7	-7.5	-3.4
$B^0 \rightarrow \eta\eta'$	0.14	0.08	0.38	1.0	2.3	0.7	0.1	0.1	0.4	-4.8	-11.4	-3.5
$B^0 \rightarrow \eta'\eta'$	0.04	0.01	0.13	0.3	2.0	0.2	0.04	0.01	0.1	-2.7	-20.2	-3.1
$B^+ \rightarrow \pi^+\eta$	3.53	2.79	1.77	0.4	0.5	1.0	3.5	2.7	1.7	-1.5	-2.1	-4.40
$B^+ \rightarrow \pi^+\eta'$	2.50	1.88	1.03	0.1	0.2	0.4	2.5	1.9	1.0	-0.9	-1.6	-4.5
$B^0 \rightarrow \pi^0\eta$	0.26	0.30	0.40	1.5	1.6	1.7	0.2	0.3	0.4	-9.0	-9.1	-8.6
$B^0 \rightarrow \pi^0\eta'$	0.06	0.08	0.15	0.9	0.9	0.7	0.05	0.1	0.1	-15.9	-16.4	-13.5
$B^+ \rightarrow K^+\pi^0$	12.3	13.8	17.1	2.4	2.3	2.2	11.2	12.5	15.4	-7.1	-7.3	-7.5
$B^0 \rightarrow K^+\pi^-$	18.0	20.0	24.2	1.3	1.3	1.2	16.2	17.9	21.6	-9.3	-9.4	-9.7
$B^+ \rightarrow K^0\pi^+$	20.2	23.6	31.1	1.4	1.5	1.6	18.1	21.2	28.0	-9.0	-8.8	-8.5
$B^0 \rightarrow K^0\pi^0$	7.28	8.33	10.7	0.1	0.2	0.5	6.4	7.4	9.5	-11.6	-11.5	-11.1
$B^+ \rightarrow K^+\eta$	3.91	4.58	6.12	0.0	0.3	0.8	3.5	4.1	5.6	-9.6	-9.3	-8.7
$B^+ \rightarrow K^+\eta'$	23.0	28.9	43.0	1.6	1.5	1.4	19.8	25.2	37.8	-12.1	-11.6	-10.8
$B^0 \rightarrow K^0\eta$	3.24	3.66	4.63	0.6	0.8	1.1	2.9	3.3	4.1	-9.9	-9.8	-9.5
$B^0 \rightarrow K^0\eta'$	22.3	28.5	43.5	1.4	1.4	1.3	19.3	24.9	38.5	-12.2	-11.5	-10.5
$B^+ \rightarrow K^+\bar{K}^0$	1.18	1.37	1.81	1.4	1.5	1.6	1.1	1.2	1.6	-8.9	-8.7	-8.4
$B^0 \rightarrow K^0\bar{K}^0$	1.11	1.30	1.71	1.4	1.5	1.6	1.0	1.2	1.5	-8.9	-8.7	-8.4

TABLE VII. $B \rightarrow PV$ branching ratios (in units of 10^{-6}) using the BSW [LQCSR] form factors in the SM, with $k^2 = m_b^2/2$, $N^{eff} = 2, 3, \infty$. The last column shows the CLEO measurements and upper limits (90% C.L.) [22-25,27].

Channel	Class	$N^{eff} = 2$	$N^{eff} = 3$	$N^{eff} = \infty$	Data
$B^0 \rightarrow \rho^+ \pi^-$	I	21.1 [25.1]	24.0 [28.5]	30.3 [36.0]	} $27.6^{+8.4}_{-7.4} \pm 4.2$
$B^0 \rightarrow \rho^- \pi^+$	I	5.7 [6.5]	6.5 [7.4]	8.2 [9.4]	
$B^0 \rightarrow \rho^0 \pi^0$	II	0.49 [0.58]	0.06 [0.07]	2.05 [2.41]	< 5.1
$B^+ \rightarrow \rho^0 \pi^+$	III	5.72 [6.63]	3.46 [3.97]	0.71 [0.78]	$10.4^{+3.3}_{-3.4} \pm 2.1$
$B^+ \rightarrow \rho^+ \pi^0$	III	13.5 [16.0]	12.6 [15.0]	10.9 [13.1]	< 43
$B^0 \rightarrow \rho^0 \eta$	II	0.01 [0.02]	0.02 [0.02]	0.06 [0.08]	< 10
$B^0 \rightarrow \rho^0 \eta'$	II	0.01 [0.01]	0.002 [0.003]	0.03 [0.03]	< 12
$B^+ \rightarrow \rho^+ \eta$	III	5.44 [6.57]	4.75 [5.79]	3.54 [4.38]	< 15
$B^+ \rightarrow \rho^+ \eta'$	III	4.35 [5.02]	3.81 [4.40]	2.85 [3.29]	< 33
$B^0 \rightarrow \omega \pi^0$	II	0.29 [0.35]	0.08 [0.09]	0.15 [0.19]	< 5.5
$B^+ \rightarrow \omega \pi^+$	III	6.32 [7.35]	3.75 [4.31]	0.78 [0.85]	$11.3^{+3.3}_{-2.9} \pm 1.4$
$B^0 \rightarrow \omega \eta$	II	0.32 [0.38]	0.03 [0.04]	0.82 [0.98]	< 12
$B^0 \rightarrow \omega \eta'$	II	0.20 [0.23]	0.001 [0.002]	0.68 [0.79]	< 60
$B^0 \rightarrow \phi \pi^0$	V	0.03 [0.04]	0.002 [0.002]	0.23 [0.27]	< 5.4
$B^+ \rightarrow \phi \pi^+$	V	0.06 [0.08]	0.004 [0.005]	0.49 [0.58]	< 4
$B^0 \rightarrow \phi \eta$	V	0.01 [0.01]	0.001 [0.001]	0.09 [0.10]	< 9
$B^0 \rightarrow \phi \eta'$	V	0.01 [0.01]	0.001 [0.001]	0.07 [0.08]	< 31
$B^+ \rightarrow \bar{K}^{*0} K^+$	IV	0.42 [0.49]	0.53 [0.61]	0.78 [0.90]	< 5.3
$B^0 \rightarrow \bar{K}^{*0} K^0$	IV	0.40 [0.46]	0.50 [0.58]	0.73 [0.89]	—
$B^+ \rightarrow K^{*+} \bar{K}^0$	V	0.005 [0.007]	0.002 [0.003]	0.001 [0.001]	—
$B^0 \rightarrow K^{*0} \bar{K}^0$	IV	0.004 [0.006]	0.002 [0.003]	0.001 [0.001]	< 12
$B^0 \rightarrow \rho^0 K^0$	IV	0.52 [0.60]	0.53 [0.62]	0.71 [0.83]	< 27
$B^+ \rightarrow \rho^0 K^+$	IV	0.39 [0.46]	0.31 [0.36]	0.31 [0.36]	< 17
$B^0 \rightarrow \rho^- K^+$	I	0.54 [0.62]	0.59 [0.68]	0.70 [0.81]	< 25
$B^+ \rightarrow \rho^+ K^0$	IV	0.11 [0.12]	0.05 [0.05]	0.01 [0.01]	< 48
$B^+ \rightarrow K^{*+} \eta$	IV	2.43 [3.12]	2.39 [3.04]	2.32 [2.89]	$26.4^{+9.6}_{-8.2} \pm 3.3$
$B^+ \rightarrow K^{*+} \eta'$	III	0.66 [1.14]	0.36 [0.61]	0.24 [0.23]	< 35
$B^0 \rightarrow K^{*0} \eta$	IV	2.32 [2.98]	2.54 [3.23]	3.06 [3.82]	$13.8^{+5.5}_{-4.6} \pm 1.6$
$B^0 \rightarrow K^{*0} \eta'$	V	0.33 [0.69]	0.09 [0.23]	0.31 [0.26]	< 20
$B^0 \rightarrow K^{*+} \pi^-$	IV	8.59 [10.2]	9.67 [11.5]	12.0 [14.3]	22^{+8+4}_{-6-5}
$B^0 \rightarrow K^{*0} \pi^0$	IV	2.44 [2.77]	3.02 [3.43]	4.42 [5.01]	< 3.6
$B^+ \rightarrow K^{*+} \pi^0$	IV	4.95 [6.09]	5.55 [6.84]	6.91 [8.52]	< 31
$B^+ \rightarrow K^{*0} \pi^+$	IV	7.35 [8.75]	9.23 [11.0]	13.6 [16.2]	< 16
$B^+ \rightarrow \phi K^+$	V	22.1 [25.7]	11.5 [13.4]	0.60 [0.70]	$17.2^{+6.7}_{-5.4} \pm 1.8$
$B^0 \rightarrow \phi K^0$	V	20.9 [24.3]	10.9 [12.6]	0.57 [0.66]	< 28
$B^0 \rightarrow \omega K^0$	V	3.31 [3.86]	0.002 [0.003]	13.3 [15.4]	< 21
$B^+ \rightarrow \omega K^+$	V	3.53 [4.11]	0.25 [0.28]	16.5 [19.2]	< 7.9

TABLE VIII. $B \rightarrow PV$ branching ratios (in units of 10^{-6}) using the BSW form factors in model III, assuming $M_{H^+} = 200\text{GeV}$, $\theta = 0^0$ and $N^{eff} = 2, 3, \infty$.

Channel	Class	SM			Model III			$\delta\mathcal{B} [\%]$		
		2	3	∞	2	3	∞	2	3	∞
$B^0 \rightarrow \rho^+ \pi^-$	I	21.1	24.0	30.3	21.2	24.1	30.5	0.7	0.7	0.7
$B^0 \rightarrow \rho^- \pi^+$	I	5.70	6.48	8.19	5.70	6.48	8.19	0.0	0.0	0.0
$B^0 \rightarrow \rho^0 \pi^0$	II	0.49	0.06	2.05	0.54	0.11	2.12	9.8	99.6	3.5
$B^+ \rightarrow \rho^0 \pi^+$	III	5.72	3.46	0.71	5.79	3.54	0.81	1.3	2.3	14.0
$B^+ \rightarrow \rho^+ \pi^0$	III	13.5	12.6	10.9	13.6	12.7	11.0	0.4	0.5	0.7
$B^0 \rightarrow \rho^0 \eta$	II	0.01	0.02	0.06	0.03	0.03	0.08	86.0	100	40.1
$B^0 \rightarrow \rho^0 \eta'$	II	0.01	0.003	0.03	0.004	0.001	0.03	-47.3	-54.4	18.1
$B^+ \rightarrow \rho^+ \eta$	III	5.44	4.75	3.54	5.46	4.79	3.59	0.5	0.7	1.4
$B^+ \rightarrow \rho^+ \eta'$	III	4.35	3.81	2.85	4.34	3.81	2.86	-0.2	-0.08	0.4
$B^0 \rightarrow \omega \pi^0$	II	0.29	0.08	0.15	0.45	0.14	0.15	54.4	77.0	0.8
$B^+ \rightarrow \omega \pi^+$	III	6.32	3.75	0.78	6.63	3.86	0.79	5.0	3.1	1.1
$B^0 \rightarrow \omega \eta$	II	0.32	0.03	0.82	0.37	0.05	0.83	16.3	67.1	0.2
$B^0 \rightarrow \omega \eta'$	II	0.20	0.001	0.68	0.22	0.004	0.69	9.5	155	0.5
$B^0 \rightarrow \phi \pi^0$	V	0.03	0.002	0.23	0.05	0.002	0.33	59.1	1.9	42.3
$B^+ \rightarrow \phi \pi^+$	V	0.06	0.004	0.49	0.10	0.004	0.69	59.1	1.9	42.3
$B^0 \rightarrow \phi \eta$	V	0.01	0.001	0.09	0.02	0.001	0.12	59.1	1.9	42.3
$B^0 \rightarrow \phi \eta'$	V	0.01	0.001	0.07	0.01	0.001	0.10	59.1	1.9	42.3
$B^+ \rightarrow \bar{K}^{*0} K^+$	IV	0.42	0.53	0.78	0.68	0.83	1.19	61.0	57.9	53.3
$B^0 \rightarrow \bar{K}^{*0} K^0$	IV	0.40	0.50	0.73	0.64	0.79	1.12	61.0	57.9	53.3
$B^+ \rightarrow K^{*+} \bar{K}^0$	V	0.005	0.002	0.001	0.002	0.001	0.003	-58.4	-72.5	256
$B^0 \rightarrow K^{*0} \bar{K}^0$	IV	0.004	0.002	0.001	0.002	0.001	0.003	-58.4	-72.5	256
$B^0 \rightarrow \rho^0 K^0$	IV	0.52	0.53	0.71	0.43	0.44	0.60	-17.1	-18.3	-16.5
$B^+ \rightarrow \rho^0 K^+$	IV	0.39	0.31	0.31	0.43	0.36	0.40	8.0	16.4	30.6
$B^0 \rightarrow \rho^- K^+$	I	0.54	0.59	0.70	0.47	0.52	0.62	-13.1	-12.7	-11.8
$B^+ \rightarrow \rho^+ K^0$	IV	0.11	0.05	0.01	0.05	0.01	0.02	-50.8	-70.1	363
$B^+ \rightarrow K^{*+} \eta$	IV	2.43	2.39	2.32	3.27	3.29	3.34	34.4	37.4	43.5
$B^+ \rightarrow K^{*+} \eta'$	III	0.66	0.36	0.24	0.31	0.24	0.65	-52.2	-34.2	170
$B^0 \rightarrow K^{*0} \eta$	IV	2.32	2.54	3.06	3.15	3.47	4.20	35.8	36.5	37.4
$B^0 \rightarrow K^{*0} \eta'$	V	0.33	0.09	0.31	0.08	0.10	0.96	-77.3	6.9	204
$B^0 \rightarrow K^{*+} \pi^-$	IV	8.59	9.67	12.0	13.6	15.4	19.1	58.6	58.8	59.3
$B^0 \rightarrow K^{*0} \pi^0$	IV	2.44	3.02	4.42	4.26	5.18	7.34	74.9	71.6	66.0
$B^+ \rightarrow K^{*+} \pi^0$	IV	4.95	5.55	6.91	7.42	8.38	10.5	49.9	50.9	52.2
$B^+ \rightarrow K^{*0} \pi^+$	IV	7.35	9.23	13.6	11.9	14.7	21.0	62.0	58.8	54.1
$B^+ \rightarrow \phi K^+$	V	22.1	11.5	0.60	35.7	19.0	1.29	61.5	65.3	113
$B^0 \rightarrow \phi K^0$	V	20.9	10.9	0.57	33.7	18.0	1.21	61.5	65.3	113
$B^0 \rightarrow \omega K^0$	V	3.31	0.002	13.3	5.33	0.01	19.4	60.9	175	46.5
$B^+ \rightarrow \omega K^+$	V	3.53	0.25	16.5	5.57	0.23	23.6	57.8	-7.7	42.9

TABLE IX. $B \rightarrow PV$ branching ratios (in units of 10^{-6}) using the BSW form factors in models I and II, assuming $M_{H^+} = 200\text{GeV}$, $\tan\beta = 2$ and $N^{eff} = 2, 3, \infty$.

Channel	Model I			$\delta\mathcal{B} [\%]$			Model II			$\delta\mathcal{B} [\%]$		
	2	3	∞	2	3	∞	2	3	∞	2	3	∞
$B^0 \rightarrow \rho^+ \pi^-$	21.1	24.0	30.3	0.0	0.0	0.0	21.1	23.9	30.2	-0.1	-0.1	-0.1
$B^0 \rightarrow \rho^- \pi^+$	5.70	6.48	8.19	-0.0	-0.0	0.0	5.70	6.48	8.19	0.0	0.0	0.0
$B^0 \rightarrow \rho^0 \pi^0$	0.49	0.06	2.05	-0.1	-0.4	0.0	0.48	0.05	2.04	-1.9	-18.9	-0.6
$B^+ \rightarrow \rho^0 \pi^+$	5.72	3.46	0.71	-0.0	-0.0	0.1	5.70	3.44	0.69	-0.3	-0.5	-2.8
$B^+ \rightarrow \rho^+ \pi^0$	13.5	12.6	10.9	0.0	0.0	0.0	13.5	12.6	10.9	-0.1	-0.1	-0.1
$B^0 \rightarrow \rho^0 \eta$	0.02	0.02	0.06	2.9	3.7	1.6	0.01	0.01	0.05	-12.8	-15.2	-6.2
$B^0 \rightarrow \rho^0 \eta'$	0.01	0.002	0.03	-0.2	-0.1	0.0	0.01	0.003	0.03	18.1	39.1	-1.1
$B^+ \rightarrow \rho^+ \eta$	5.44	4.76	3.54	0.0	0.0	0.1	5.43	4.75	3.53	-0.1	-0.1	-0.2
$B^+ \rightarrow \rho^+ \eta'$	4.35	3.81	2.85	-0.0	-0.0	0.0	4.36	3.81	2.85	0.1	0.1	-0.0
$B^0 \rightarrow \omega \pi^0$	0.29	0.08	0.15	0.2	-0.4	0.5	0.26	0.07	0.15	-10.7	-15.4	0.4
$B^+ \rightarrow \omega \pi^+$	6.33	3.75	0.78	0.1	0.1	0.0	6.26	3.73	0.78	-0.9	-0.5	-0.2
$B^0 \rightarrow \omega \eta$	0.32	0.03	0.82	0.7	3.6	0.0	0.31	0.03	0.82	-2.7	-9.9	-0.1
$B^0 \rightarrow \omega \eta'$	0.209	0.001	0.68	0.2	0.3	0.1	0.20	0.002	0.68	-1.3	8.7	-0.1
$B^0 \rightarrow \phi \pi^0$	0.03	0.002	0.23	-0.8	10.9	2.4	0.03	0.002	0.21	-12.9	10.9	-6.7
$B^+ \rightarrow \phi \pi^+$	0.06	0.004	0.50	-0.8	10.9	2.4	0.06	0.005	0.45	-12.9	10.9	-6.7
$B^0 \rightarrow \phi \eta$	0.01	0.001	0.09	-0.8	10.9	2.4	0.01	0.001	0.08	-12.9	10.9	-6.7
$B^0 \rightarrow \phi \eta'$	0.01	0.001	0.07	-0.8	10.9	2.4	0.01	0.001	0.06	-12.9	10.9	-6.7
$B^+ \rightarrow \bar{K}^{*0} K^+$	0.43	0.54	0.79	1.8	1.9	2.1	0.37	0.47	0.71	-10.7	-10.0	-9.0
$B^0 \rightarrow \bar{K}^{*0} K^0$	0.40	0.51	0.75	1.8	1.9	2.1	0.35	0.45	0.67	-10.7	-10.0	-9.0
$B^+ \rightarrow K^{*+} \bar{K}^0$	0.005	0.002	0.001	-3.5	-7.1	13.5	0.01	0.002	0.001	14.3	20.9	-16.6
$B^0 \rightarrow K^{*0} \bar{K}^0$	0.004	0.002	0.001	-3.5	-7.1	13.5	0.005	0.002	0.001	14.3	20.9	-16.6
$B^0 \rightarrow \rho^0 K^0$	0.53	0.55	0.74	3.1	3.3	3.1	0.56	0.58	0.77	7.6	8.2	7.6
$B^+ \rightarrow \rho^0 K^+$	0.40	0.32	0.34	2.4	4.9	9.0	0.40	0.31	0.32	0.7	1.4	2.4
$B^0 \rightarrow \rho^- K^+$	0.53	0.58	0.70	-1.8	-1.4	-0.6	0.55	0.60	0.72	1.6	2.0	2.7
$B^+ \rightarrow \rho^+ K^0$	0.10	0.04	0.005	-3.0	-6.3	11.6	0.12	0.05	0.005	11.6	16.7	-6.5
$B^+ \rightarrow K^{*+} \eta$	2.49	2.45	2.36	2.5	2.3	1.7	2.31	2.26	2.15	-4.9	-5.8	-7.5
$B^+ \rightarrow K^{*+} \eta'$	0.64	0.35	0.24	-2.4	-2.3	2.0	0.77	0.43	0.21	16.6	19.5	-12.5
$B^0 \rightarrow K^{*0} \eta$	2.37	2.60	3.13	2.4	2.3	2.2	2.19	2.40	2.88	-5.4	-5.6	-5.9
$B^0 \rightarrow K^{*0} \eta'$	0.32	0.09	0.33	-3.3	-4.7	5.0	0.42	0.13	0.23	27.3	42.6	-25.4
$B^0 \rightarrow K^{*+} \pi^-$	8.76	9.84	12.2	2.0	1.8	1.4	7.74	8.69	10.8	-9.8	-10.1	-10.5
$B^0 \rightarrow K^{*0} \pi^0$	2.44	3.03	4.45	0.1	0.4	0.8	2.08	2.60	3.87	-14.7	-13.9	-12.5
$B^+ \rightarrow K^{*+} \pi^0$	5.11	5.72	7.10	3.2	3.0	2.7	4.60	5.14	6.35	-7.2	-7.5	-8.1
$B^+ \rightarrow K^{*0} \pi^+$	7.48	9.41	13.9	1.8	1.9	2.1	6.55	8.29	12.4	-10.8	-10.2	-9.2
$B^+ \rightarrow \phi K^+$	22.3	11.6	0.61	1.1	1.0	0.7	19.5	10.1	0.48	-11.5	-12.2	-19.9
$B^0 \rightarrow \phi K^0$	21.1	11.0	0.57	1.1	1.0	0.7	18.5	9.54	0.46	-11.5	-12.2	-19.9
$B^0 \rightarrow \omega K^0$	3.35	0.002	13.4	1.2	1.1	1.3	2.94	0.003	12.1	-11.3	25.7	-8.5
$B^+ \rightarrow \omega K^+$	3.59	0.25	16.7	1.6	-0.1	1.4	3.17	0.25	15.2	-10.1	2.3	-7.7

TABLE X. $B \rightarrow VV$ branching ratios (in units of 10^{-6}) using the BSW [LQQR] form factors in the SM, with $k^2 = m_b^2/2$, $N^{eff} = 2, 3, \infty$. The last column shows the CLEO upper limits (90% C.L.) [22-25].

Channel	Class	$N^{eff} = 2$	$N^{eff} = 3$	$N^{eff} = \infty$	Data
$B^0 \rightarrow \rho^+ \rho^-$	I	17.8 [19.8]	20.2 [22.5]	25.5 [28.4]	< 2200
$B^0 \rightarrow \rho^0 \rho^0$	II	0.39 [0.44]	0.09 [0.10]	1.56 [1.73]	< 4.8
$B^0 \rightarrow \omega \omega$	II	0.81 [0.90]	0.15 [0.17]	1.22 [1.35]	< 19
$B^+ \rightarrow \rho^+ \rho^0$	III	12.8 [14.3]	10.1 [11.3]	5.69 [6.33]	< 120
$B^+ \rightarrow \rho^+ \omega$	III	15.7 [17.4]	12.2 [13.5]	6.69 [7.45]	< 47
$B^0 \rightarrow K^{*+} \rho^-$	IV	6.17 [6.82]	6.95 [7.68]	8.64 [9.55]	—
$B^0 \rightarrow K^{*0} \rho^0$	IV	1.73 [1.82]	2.01 [2.11]	2.79 [2.91]	< 16.1
$B^+ \rightarrow K^{*+} \rho^0$	IV	5.22 [5.97]	5.97 [6.82]	7.76 [8.91]	< 52
$B^+ \rightarrow K^{*0} \rho^+$	IV	6.65 [7.35]	8.36 [9.24]	12.4 [13.7]	—
$B^+ \rightarrow K^{*+} \bar{K}^{*0}$	IV	0.38 [0.49]	0.48 [0.61]	0.70 [0.90]	< 62
$B^0 \rightarrow K^{*0} \bar{K}^{*0}$	IV	0.36 [0.47]	0.46 [0.58]	0.67 [0.86]	< 7.4
$B^0 \rightarrow \rho^0 \omega$	V	0.45 [0.50]	0.24 [0.27]	0.02 [0.02]	< 11
$B^0 \rightarrow K^{*0} \omega$	V	13.5 [16.1]	4.52 [5.03]	1.04 [1.79]	< 19
$B^+ \rightarrow K^{*+} \omega$	V	13.4 [16.1]	3.94 [4.39]	2.74 [4.01]	< 52
$B^+ \rightarrow K^{*+} \phi$	V	21.8 [27.8]	11.3 [14.5]	0.60 [0.76]	< 41
$B^0 \rightarrow K^{*0} \phi$	V	20.6 [26.2]	10.7 [13.6]	0.56 [0.72]	< 21
$B^+ \rightarrow \rho^+ \phi$	V	0.06 [0.07]	0.004 [0.005]	0.47 [0.52]	< 16
$B^0 \rightarrow \rho^0 \phi$	V	0.03 [0.03]	0.001 [0.002]	0.22 [0.25]	< 13
$B^0 \rightarrow \omega \phi$	V	0.03 [0.03]	0.001 [0.002]	0.22 [0.24]	< 21

TABLE XI. $B \rightarrow VV$ branching ratios (in units of 10^{-6}) using the BSW form factors in model III, assuming $M_{H^+} = 200\text{GeV}$, $N^{eff} = 2, 3, \infty$ and $\theta = 0^0, 30^0$.

Channel	$\theta = 0^0$			$\delta\mathcal{B} [\%]$			$\theta = 30^0$			$\delta\mathcal{B} [\%]$		
	2	3	∞	2	3	∞	2	3	∞	2	3	∞
$B^0 \rightarrow \rho^+ \rho^-$	17.9	20.3	25.7	0.7	0.7	0.7	19.3	19.7	24.8	-2.6	-2.6	-2.6
$B^0 \rightarrow \rho^0 \rho^0$	0.46	0.16	1.65	16	79	5.7	0.56	0.15	1.50	28	67	-4.0
$B^0 \rightarrow \omega \omega$	1.05	0.24	1.23	29	54	1.0	1.02	0.22	1.19	14	45	-2.3
$B^+ \rightarrow \rho^+ \rho^0$	12.8	10.1	5.69	0.0	0.0	0.0	14.3	10.1	5.69	0.0	0.0	0.0
$B^+ \rightarrow \rho^+ \omega$	13.8	10.9	6.12	-12	-11	-8.5	15.2	10.9	6.12	-13	-11	-8.5
$B^0 \rightarrow K^{*+} \rho^-$	9.78	11.0	13.8	59	59	59	11.1	11.3	14.1	62	63	63
$B^0 \rightarrow K^{*0} \rho^0$	3.18	3.70	4.98	84	84	78	3.14	3.50	4.90	72	74	75
$B^+ \rightarrow K^{*+} \rho^0$	7.61	8.75	11.4	46	47	47	8.79	8.80	11.3	47	48	45
$B^+ \rightarrow K^{*0} \rho^+$	10.8	13.3	19.0	62	59	54	11.4	12.7	18.2	55	52	48
$B^+ \rightarrow K^{*+} \bar{K}^{*0}$	0.61	0.75	1.08	61	58	53	0.73	0.71	1.02	51	49	45
$B^0 \rightarrow K^{*0} \bar{K}^{*0}$	0.59	0.72	1.03	61	58	53	0.70	0.68	0.98	51	49	45
$B^0 \rightarrow \rho^0 \omega$	0.72	0.39	0.04	61	65	79	0.76	0.37	0.03	53	54	51
$B^0 \rightarrow K^{*0} \omega$	20.8	6.97	1.51	53	54	45	23.5	6.58	1.49	46	46	44
$B^+ \rightarrow K^{*+} \omega$	20.8	6.23	3.47	55	58	27	24.3	6.25	3.24	51	59	18
$B^+ \rightarrow K^{*+} \phi$	35.2	18.8	1.27	62	65	114	42.9	17.9	1.20	54	58	101
$B^0 \rightarrow K^{*0} \phi$	33.2	17.7	1.20	62	65	113	40.4	16.9	1.13	54	58	101
$B^+ \rightarrow \rho^+ \phi$	0.10	0.004	0.67	59	1.9	42	0.10	0.004	0.64	50	1.9	36
$B^0 \rightarrow \rho^0 \phi$	0.05	0.002	0.32	59	1.9	42	0.05	0.002	0.30	50	1.9	36
$B^0 \rightarrow \omega \phi$	0.05	0.002	0.32	59	1.9	42	0.05	0.002	0.30	50	1.9	36

TABLE XII. $B \rightarrow VV$ branching ratios (in units of 10^{-6}) using the BSW form factors in models I and II, assuming $M_{H^+} = 200\text{GeV}$, $N^{eff} = 2, 3, \infty$ and $\tan\beta = 2$.

Channel	model I			$\delta\mathcal{B}$ [%]			model II			$\delta\mathcal{B}$ [%]		
	2	3	∞	2	3	∞	2	3	∞	2	3	∞
$B^0 \rightarrow \rho^+ \rho^-$	17.7	19.8	24.4	0.0	0.0	0.0	17.7	20.2	24.3	-0.1	-0.1	-0.1
$B^0 \rightarrow \rho^0 \rho^0$	0.53	0.10	1.21	0.1	0.6	0.1	0.52	0.08	1.20	-1.8	-15	-1.1
$B^0 \rightarrow \omega \omega$	0.90	0.16	0.93	0.6	1.1	0.0	0.86	0.14	0.93	-4.2	-9.9	-0.2
$B^+ \rightarrow \rho^+ \rho^0$	13.5	10.7	6.04	0.0	0.0	0.0	13.6	10.1	6.04	2.1	0.0	0.0
$B^+ \rightarrow \rho^+ \omega$	14.6	11.6	6.50	-10.9	-9.6	-7.4	14.6	10.9	6.50	-11	-11	-7.4
$B^0 \rightarrow K^{*+} \rho^-$	6.42	7.13	8.66	2.1	1.9	1.6	5.70	6.25	7.71	-9.3	-10	-9.6
$B^0 \rightarrow K^{*0} \rho^0$	1.70	1.97	2.72	0.3	0.5	0.7	1.47	1.70	2.36	-13	-16	-13
$B^+ \rightarrow K^{*+} \rho^0$	5.44	6.08	7.63	2.8	2.8	2.7	4.90	5.55	6.83	-7.5	-7.0	-8.0
$B^+ \rightarrow K^{*0} \rho^+$	6.55	8.13	11.8	1.8	1.9	2.1	5.78	7.51	10.5	-10	-10	-9.3
$B^+ \rightarrow K^{*+} \bar{K}^{*0}$	0.37	0.46	0.67	1.8	1.9	2.1	0.33	0.43	0.60	-10	-10	-9.1
$B^0 \rightarrow K^{*0} \bar{K}^{*0}$	0.35	0.45	0.65	1.8	1.9	2.1	0.32	0.41	0.57	-10	-10	-9.1
$B^0 \rightarrow \rho^0 \omega$	0.41	0.23	0.02	1.1	1.0	0.4	0.37	0.21	0.02	-10	-12	-12
$B^0 \rightarrow K^{*0} \omega$	12.3	4.15	0.92	1.3	1.3	1.3	11.1	4.07	0.83	-9.3	-9.9	-8.2
$B^+ \rightarrow K^{*+} \omega$	12.6	3.85	2.39	1.6	1.4	1.6	11.3	3.52	2.24	-9.4	-11	-4.9
$B^+ \rightarrow K^{*+} \phi$	20.4	10.8	0.65	1.4	1.4	2.2	18.0	10.0	0.54	-11	-12	-16
$B^0 \rightarrow K^{*0} \phi$	19.2	10.1	0.61	1.1	1.0	0.5	17.0	9.41	0.51	-11	-12	-16
$B^+ \rightarrow \rho^+ \phi$	0.1	0.01	0.44	-0.7	9.7	2.4	0.05	0.005	0.40	-11	11	-7.5
$B^0 \rightarrow \rho^0 \phi$	0.02	0.002	0.21	-0.7	9.7	2.4	0.02	0.002	0.19	-11	11	-7.5
$B^0 \rightarrow \omega \phi$	0.02	0.002	0.21	-0.7	9.7	2.4	0.02	0.002	0.19	-11	11	-7.5

FIGURES

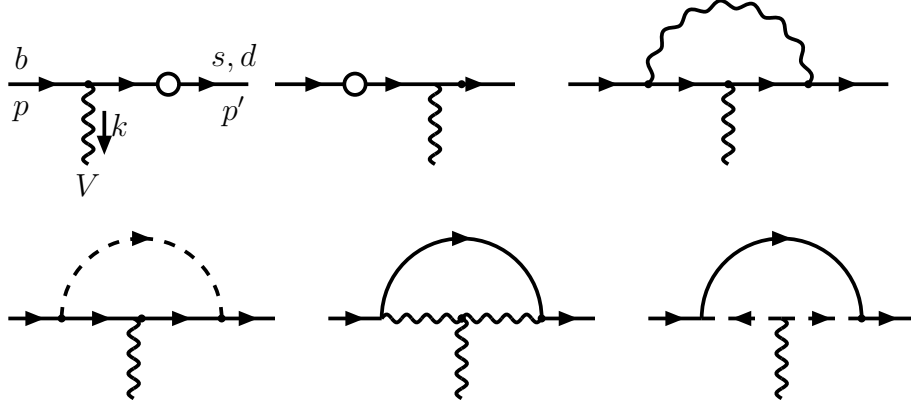


FIG. 1. Typical one-loop Feynman diagrams for the quark level decays $b \rightarrow (s,d)V^*$ ($V = \gamma, Z^0, g$), with W^\pm (internal wave lines) and charged-Higgs exchanges (internal dash lines) in the SM and two-Higgs-doublet models. The internal quarks are the upper type quark u, c and t .

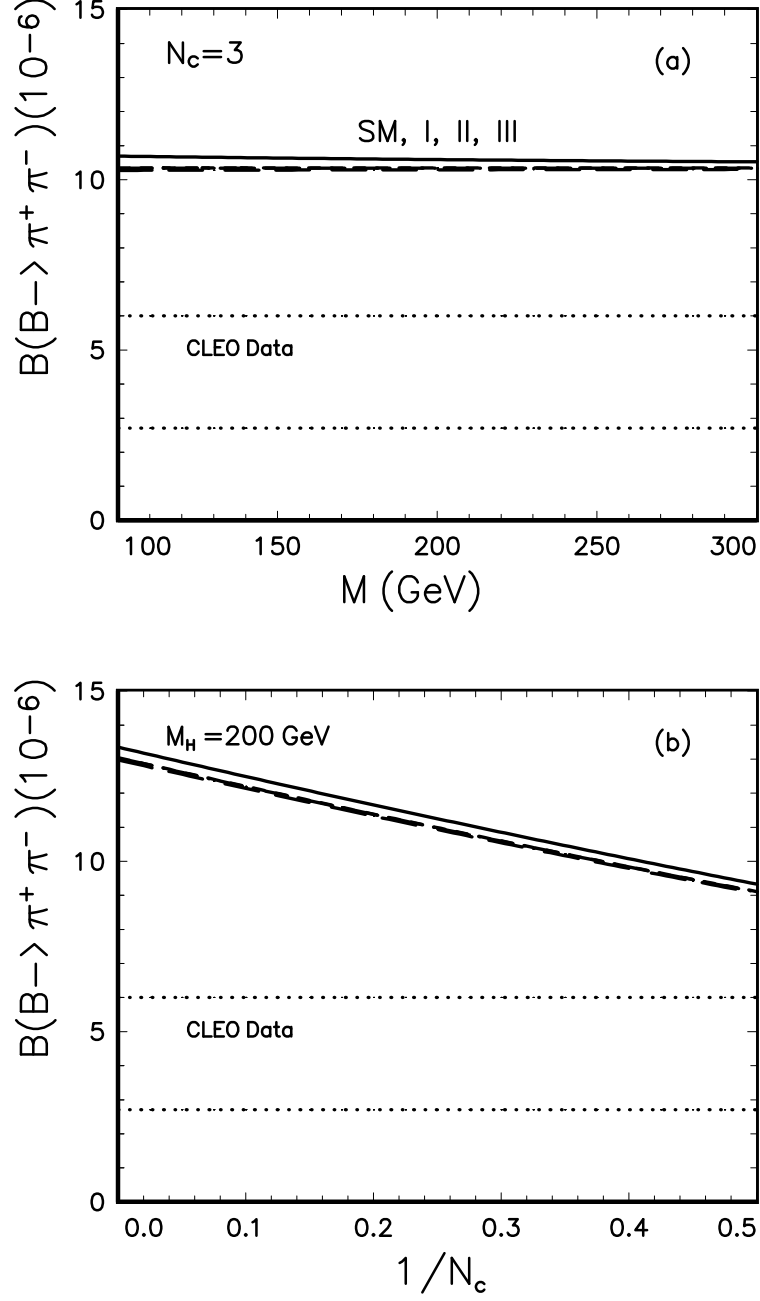


FIG. 2. Branching ratios $\mathcal{B}(B \rightarrow \pi^+ \pi^-)$ versus M_{H^+} and $1/N^{eff}$ in the SM and 2HDM's. For (a) and (b), we set $N^{eff} = 3$ and $M_{H^+} = 200\text{GeV}$, respectively. The four adjacent curves are the theoretical predictions in the SM and models I, II and III respectively. The band between two dots lines show the CLEO data with 1σ error: $\mathcal{B}(B \rightarrow \pi^+ \pi^-) = (4.3^{+1.7}_{-1.6}) \times 10^{-6}$.

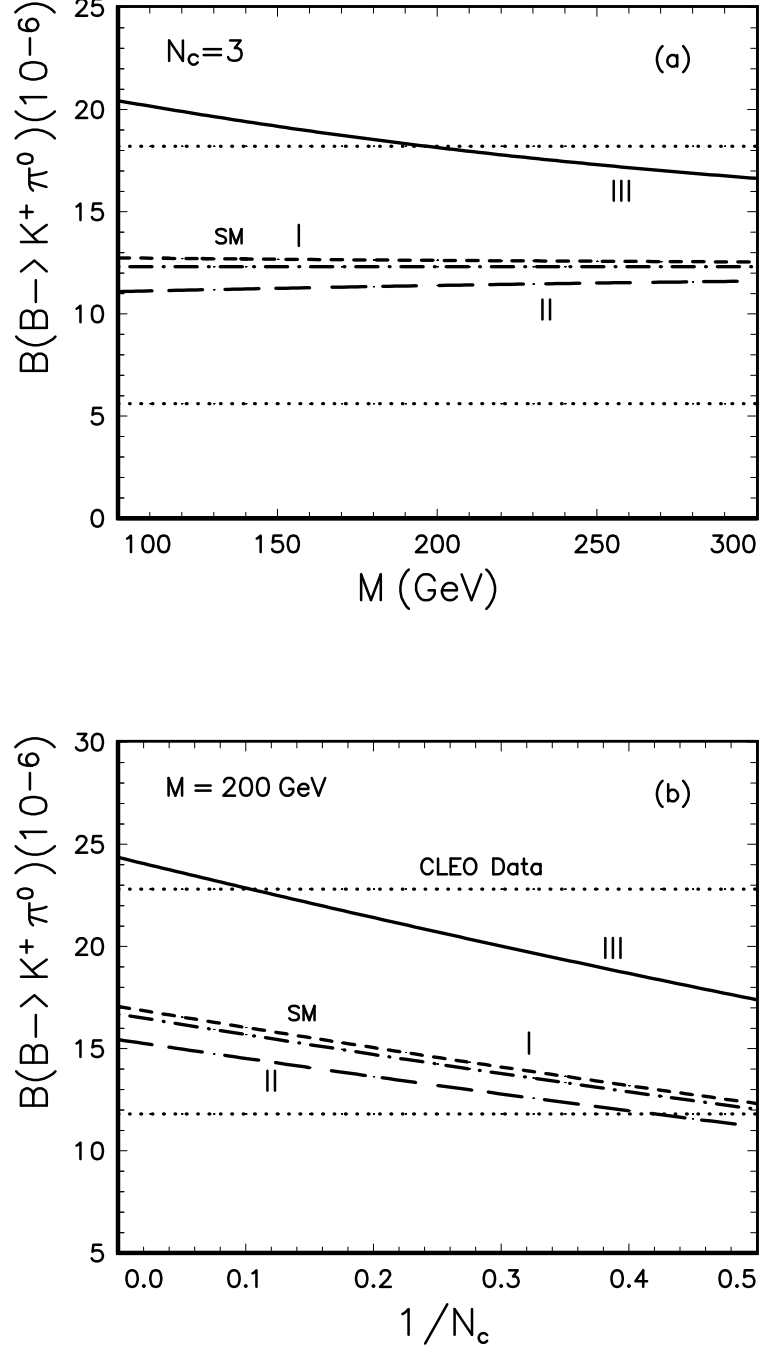


FIG. 3. Branching ratios $\mathcal{B}(B \rightarrow K^+ \pi^0)$ versus M_{H^+} and $1/N_c^{eff}$ in the SM and 2HDM's. For (a) and (b), we set $N_c^{eff} = 3$ and $M_{H^+} = 200$ GeV, respectively. The dot-dashed, short-dashed, long-dashed and solid curve corresponds to the theoretical predictions in the SM and models I, II and III, respectively. The theoretical uncertainties are not shown here. The band between two dots lines shows the CLEO data with 2σ errors: $\mathcal{B}(B \rightarrow K^+ \pi^0) = (11.6_{-6.0}^{+6.6}) \times 10^{-6}$.

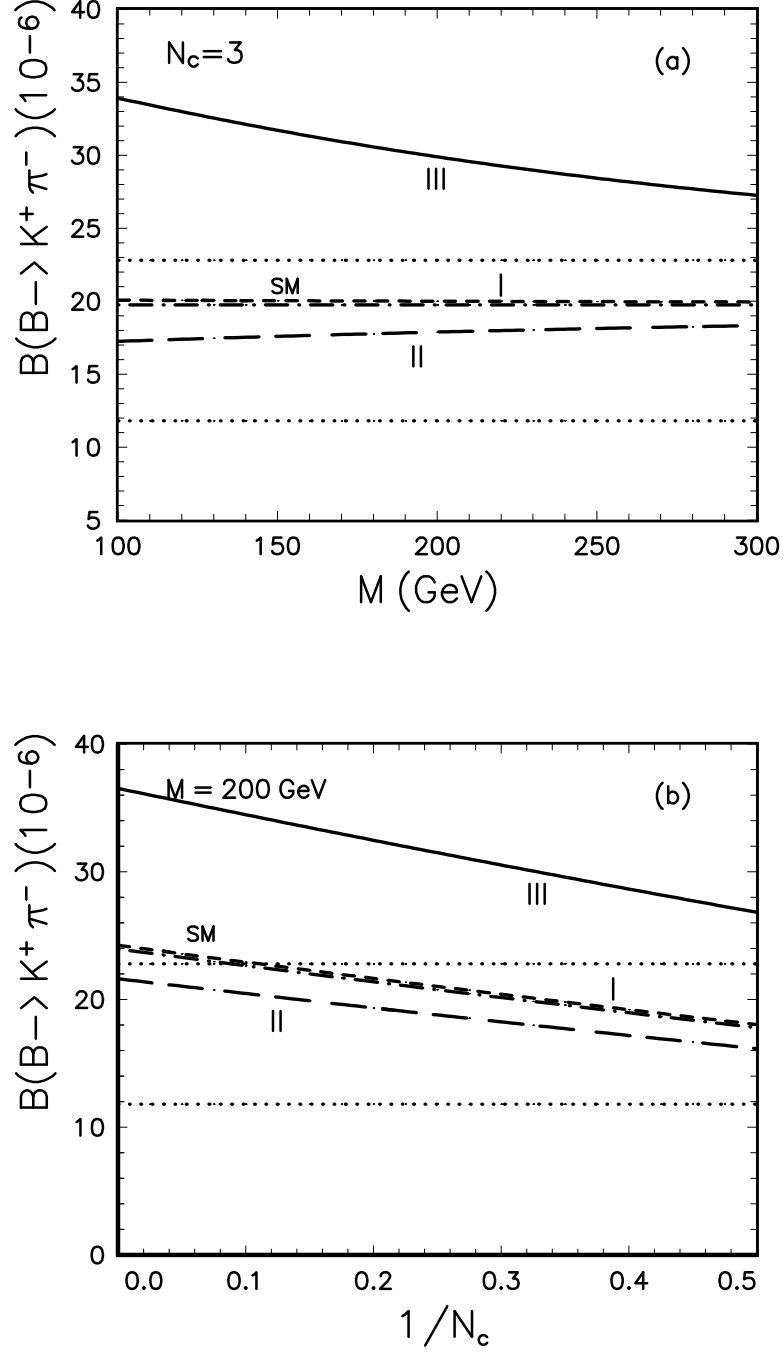


FIG. 4. Same as Fig.3, but for the decay $B \rightarrow K^+ \pi^-$. The dots band corresponds to the CLEO data with 2σ errors: $\mathcal{B}(B \rightarrow K^+ \pi^-) = (17.2^{+5.6}_{-5.4}) \times 10^{-6}$.

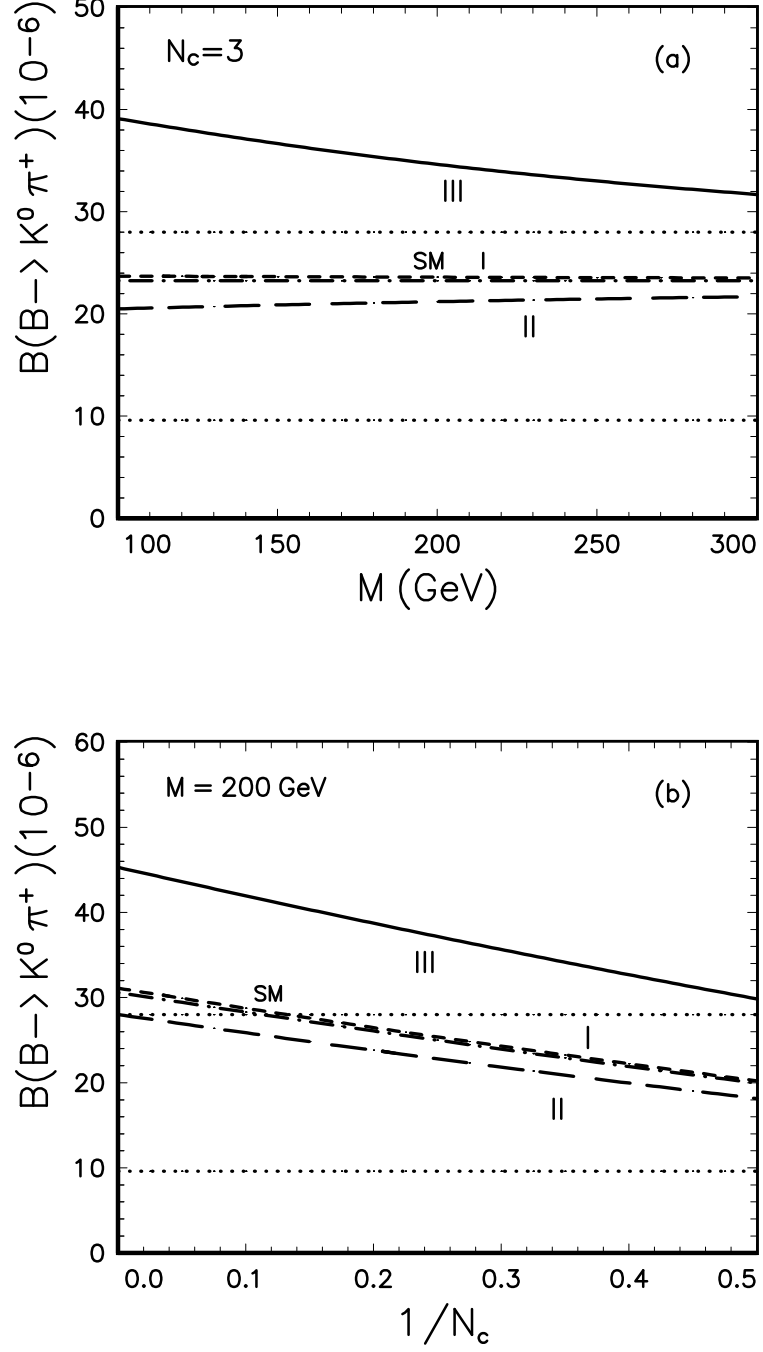


FIG. 5. Same as Fig.3, but for the decay $B \rightarrow K^0 \pi^+$. The dots band corresponds to the CLEO data with 2σ errors: $\mathcal{B}(B \rightarrow K^0 \pi^+) = (18.2^{+9.8}_{-8.6}) \times 10^{-6}$.

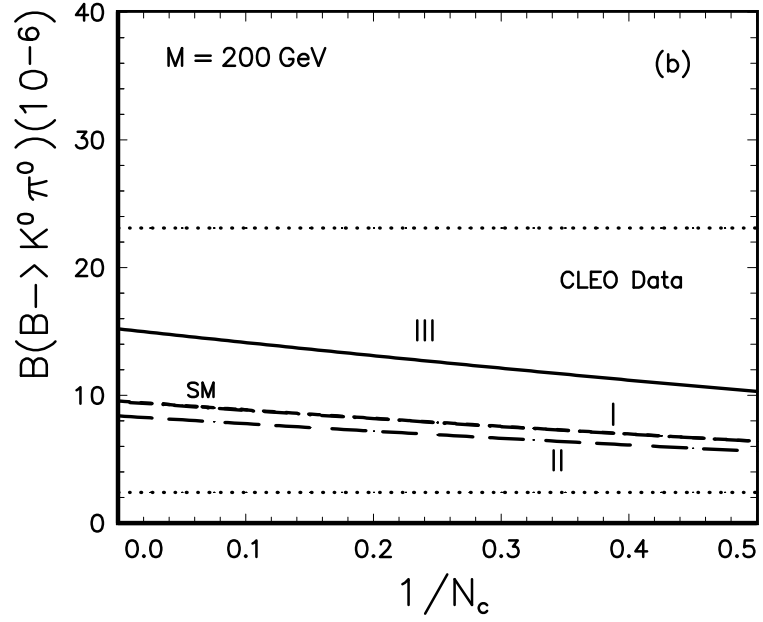
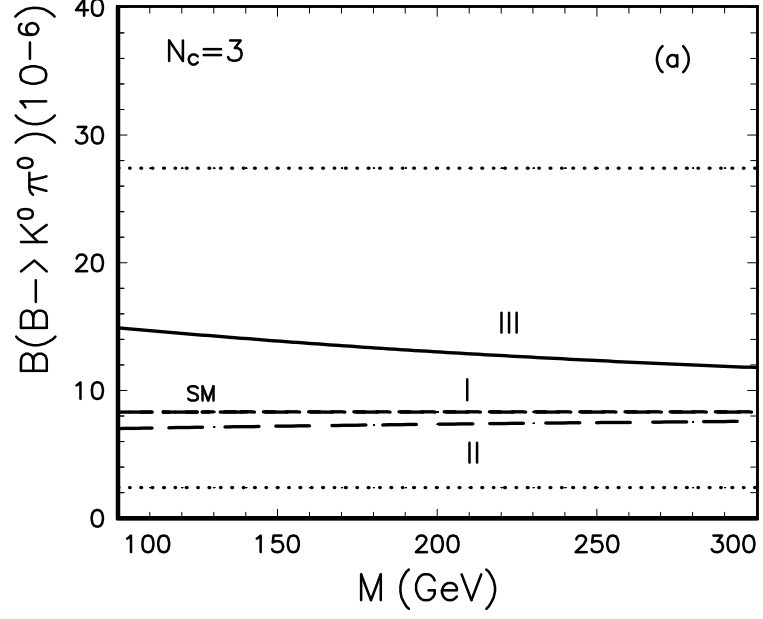


FIG. 6. Same as Fig.3, but for the decay $B \rightarrow K^0 \pi^0$. The dots band corresponds to the CLEO data with 1σ error: $\mathcal{B}(B \rightarrow K^0 \pi^0) = (14.6^{+6.4}_{-6.1}) \times 10^{-6}$.

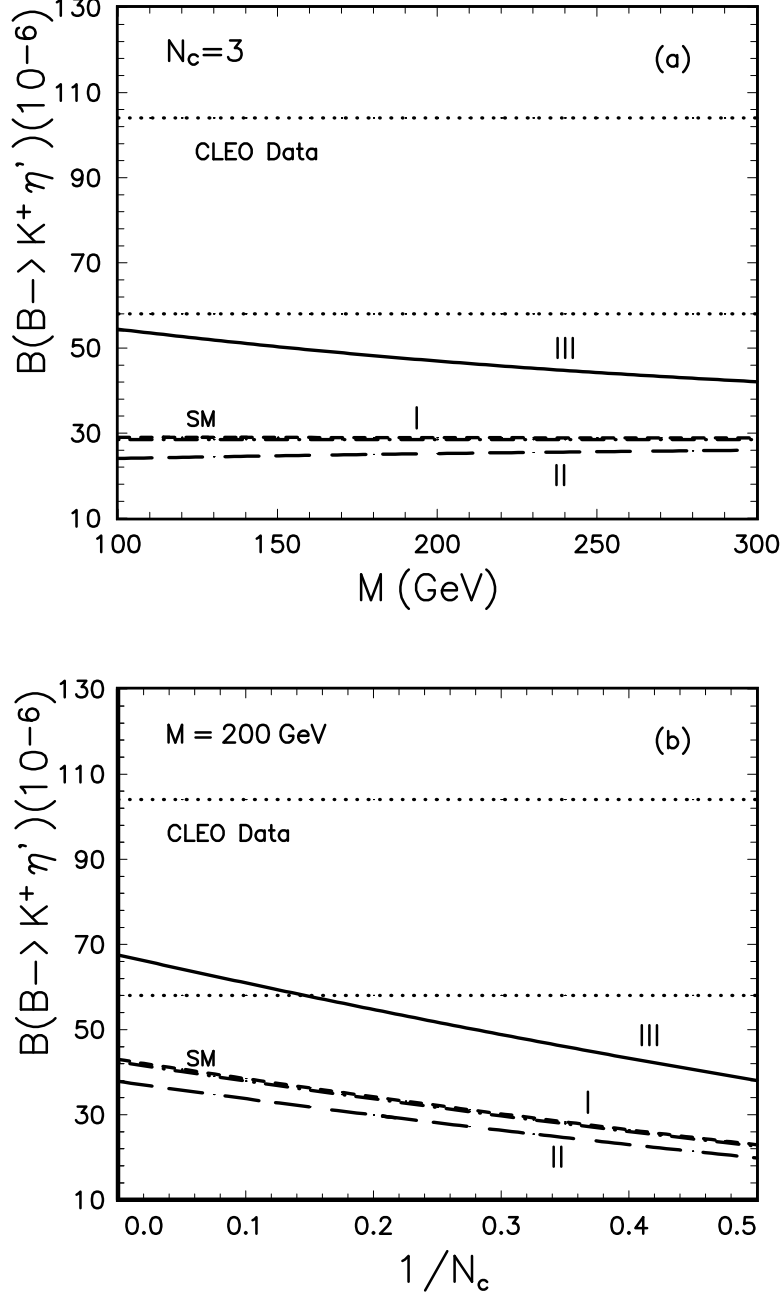


FIG. 7. Plots of $\mathcal{B}(B^+ \rightarrow K^+ \eta')$ versus M_{H^+} and $1/N^{eff}$ in the SM and 2HDM's. For (a) and (b), we set $N^{eff} = 3$ and $M_{H^+} = 200 \text{ GeV}$, respectively. The dot-dashed and the closely adjacent short-dashed curve refers to the theoretical predictions in the SM and model I; while the long-dashed and solid curve corresponds to the theoretical predictions in models II and III, respectively. The theoretical uncertainties are not shown here. The dots band corresponds to the CLEO data with 2σ errors: $\mathcal{B}(B^+ \rightarrow K^+ \eta') = (80^{+24}_{-22}) \times 10^{-6}$.

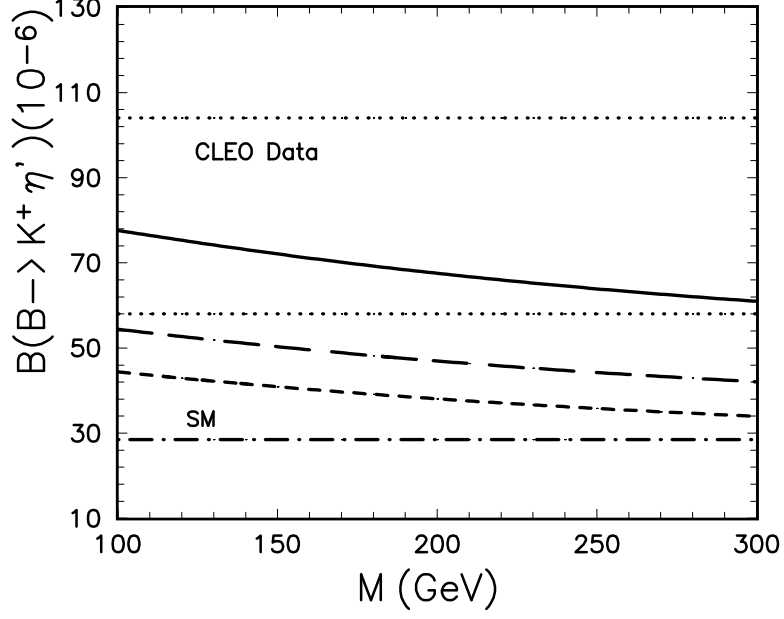


FIG. 8. Plots of $\mathcal{B}(B^+ \rightarrow K^+ \eta')$ versus M_{H^+} in the SM and model III. The dot-dashed line shows the SM prediction with $N^{eff} = 3$. The short-dashed, long-dashed and solid curve corresponds to model III predictions for $N^{eff} = 2, 3, \infty$, respectively. Other theoretical uncertainties are not shown here. The dots band corresponds to the CLEO data with 2σ errors: $\mathcal{B}(B^+ \rightarrow K^+ \eta') = (80^{+24}_{-22}) \times 10^{-6}$.

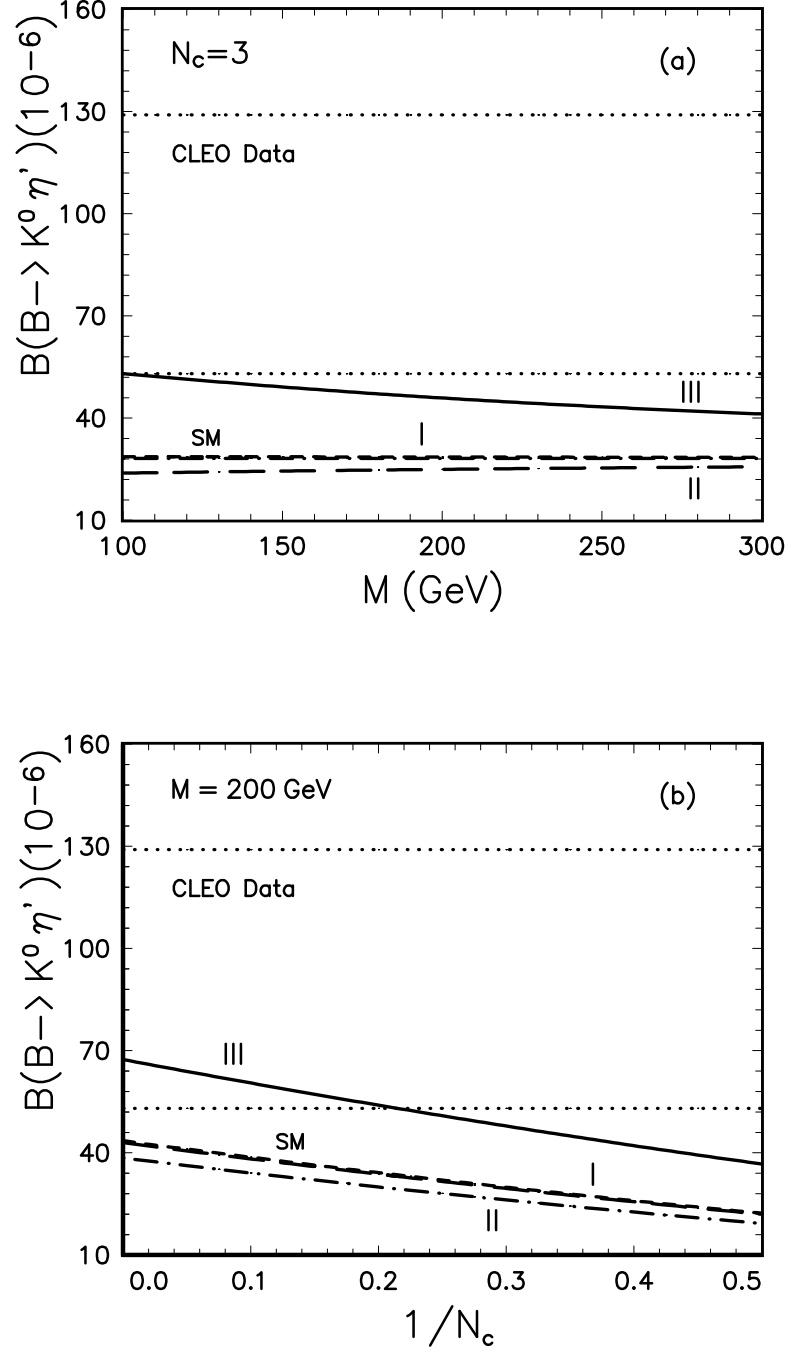


FIG. 9. Same as Fig.3, but for the decay $B \rightarrow K^0 \eta'$. The dots band corresponds to the CLEO data with 2σ errors: $\mathcal{B}(B^0 \rightarrow K^0 \eta') = (89^{+40}_{-36}) \times 10^{-6}$.

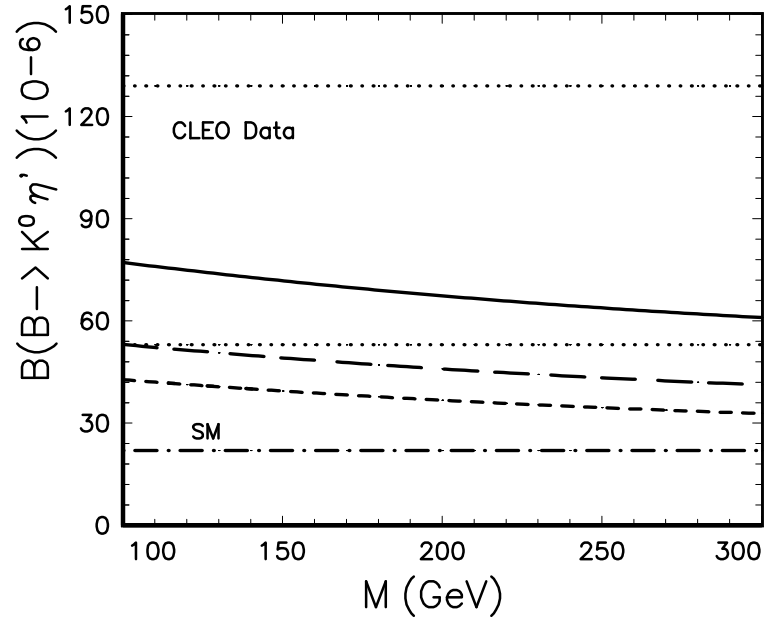


FIG. 10. Same as Fig.8, but for the decay $B \rightarrow K^0 \eta'$. The dots band corresponds to the CLEO data with 2σ errors: $\mathcal{B}(B^0 \rightarrow K^0 \eta') = (89^{+40}_{-36}) \times 10^{-6}$.

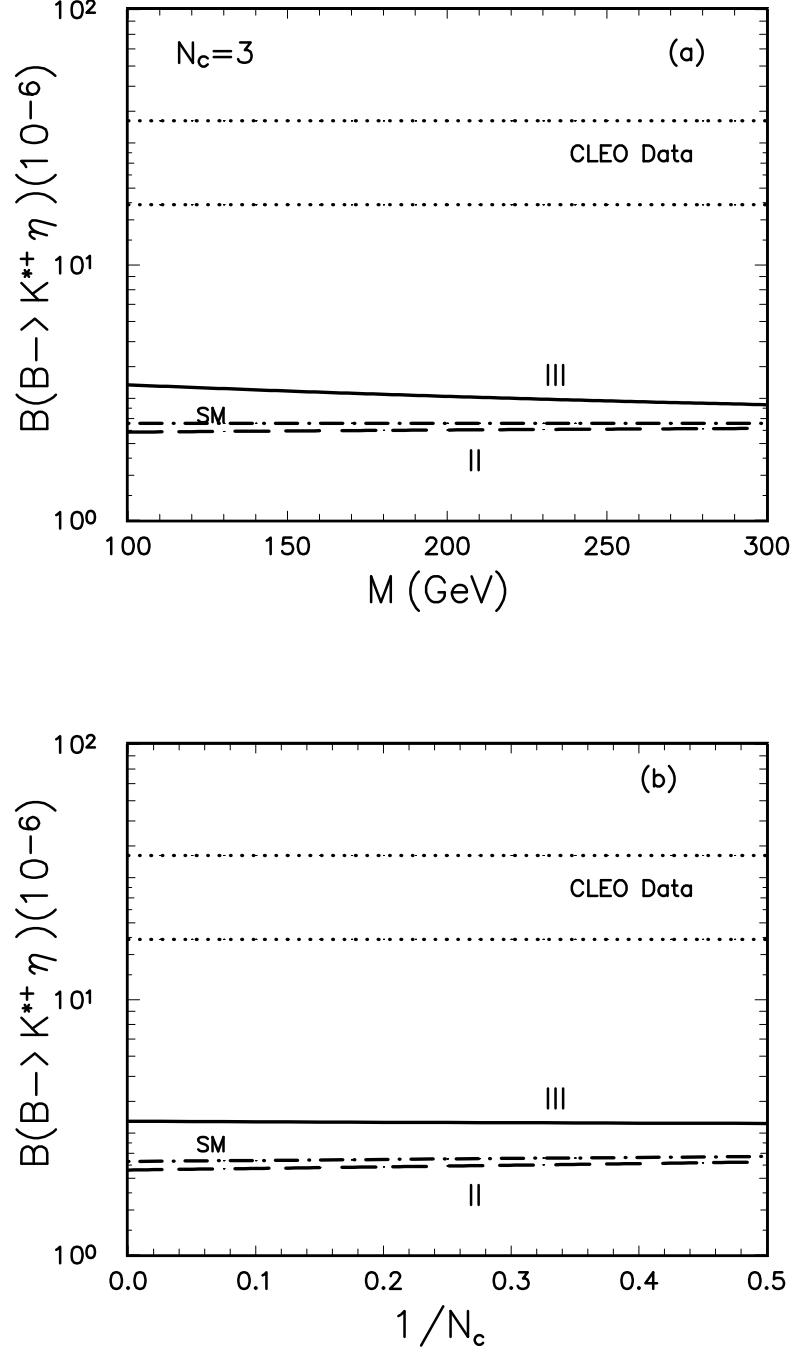


FIG. 11. $\mathcal{B}(B \rightarrow K^{*+} \eta)$ versus M_{H^+} and $1/N_c^{eff}$ in the SM and 2HDM's. For (a) and (b), we set $N_c^{eff} = 3$ and $M_{H^+} = 200 \text{ GeV}$, respectively. The dot-dashed, long-dashed and solid curve shows the theoretical predictions in the SM and models II and III, respectively. The theoretical uncertainties are not shown here. The dots band corresponds to the CLEO data with 1σ error: $\mathcal{B}(B^+ \rightarrow K^{*+} \eta) = (26.4_{-8.8}^{+10.2}) \times 10^{-6}$.

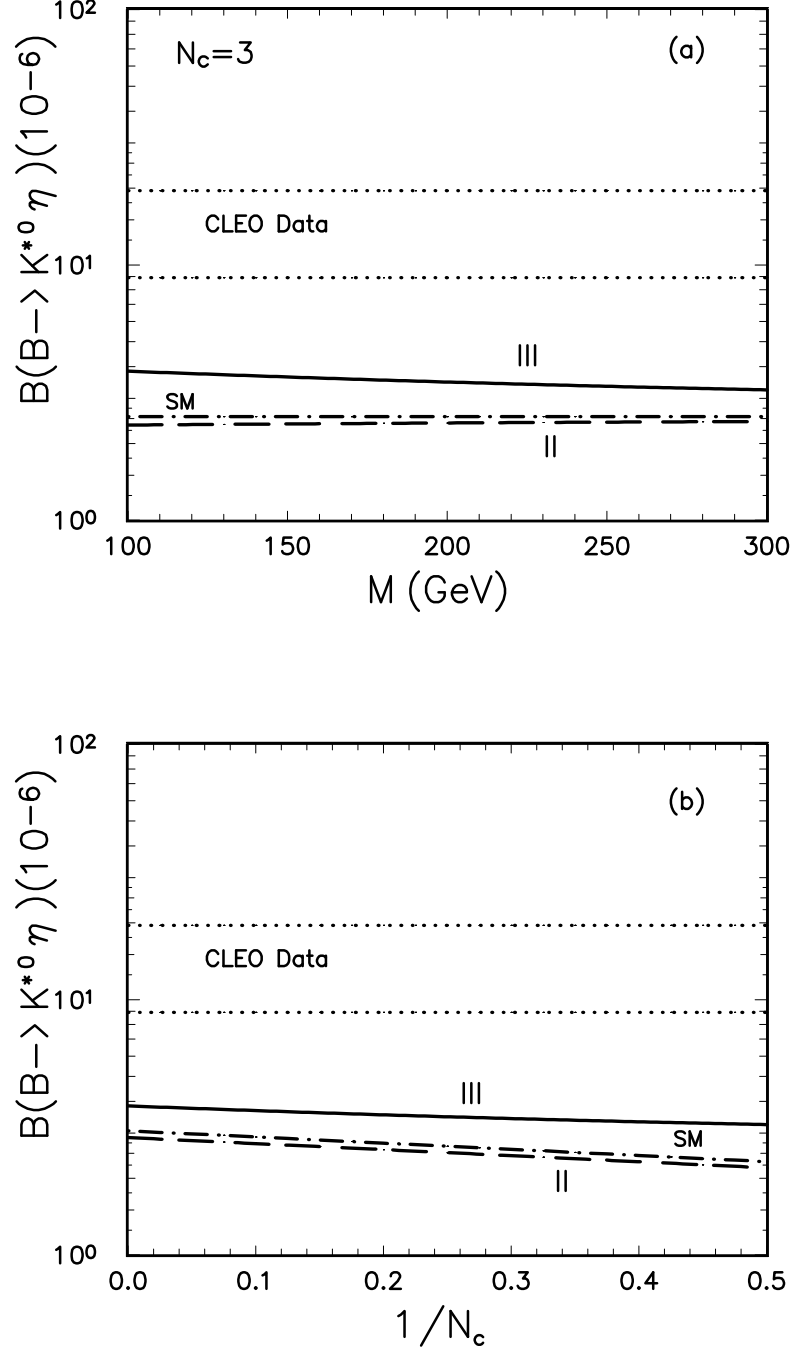


FIG. 12. Same as Fig.11, but for the decay $B \rightarrow K^{*0} \eta$. The dots band corresponds to the CLEO data with 1σ error: $\mathcal{B}(B^0 \rightarrow K^{*0} \eta) = (13.8^{+5.7}_{-4.9}) \times 10^{-6}$.

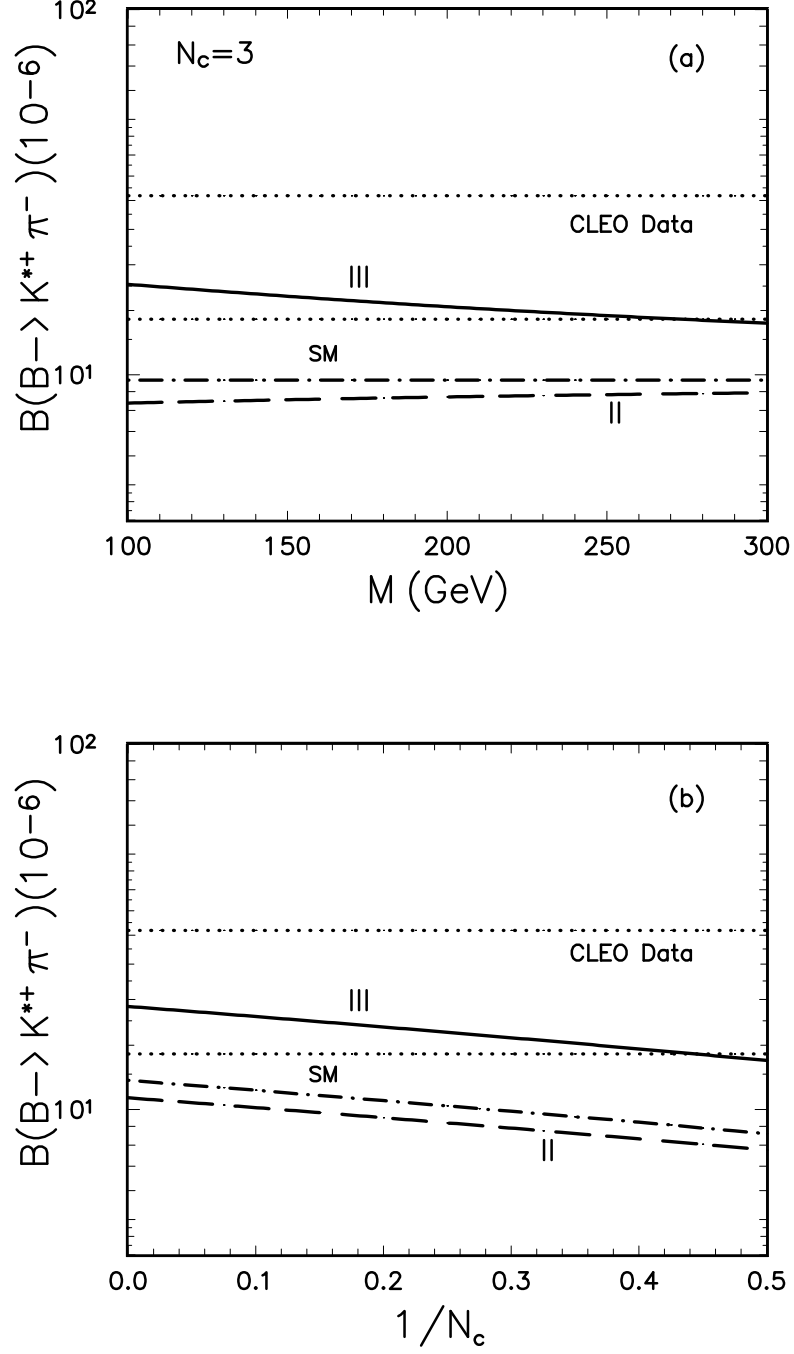


FIG. 13. Same as Fig.11, but for the decay $B \rightarrow K^{*+} \pi^-$. The dots band corresponds to the CLEO data with 1σ error: $\mathcal{B}(B^0 \rightarrow K^{*+} \pi^-) = (22^{+8.9}_{-7.8}) \times 10^{-6}$.

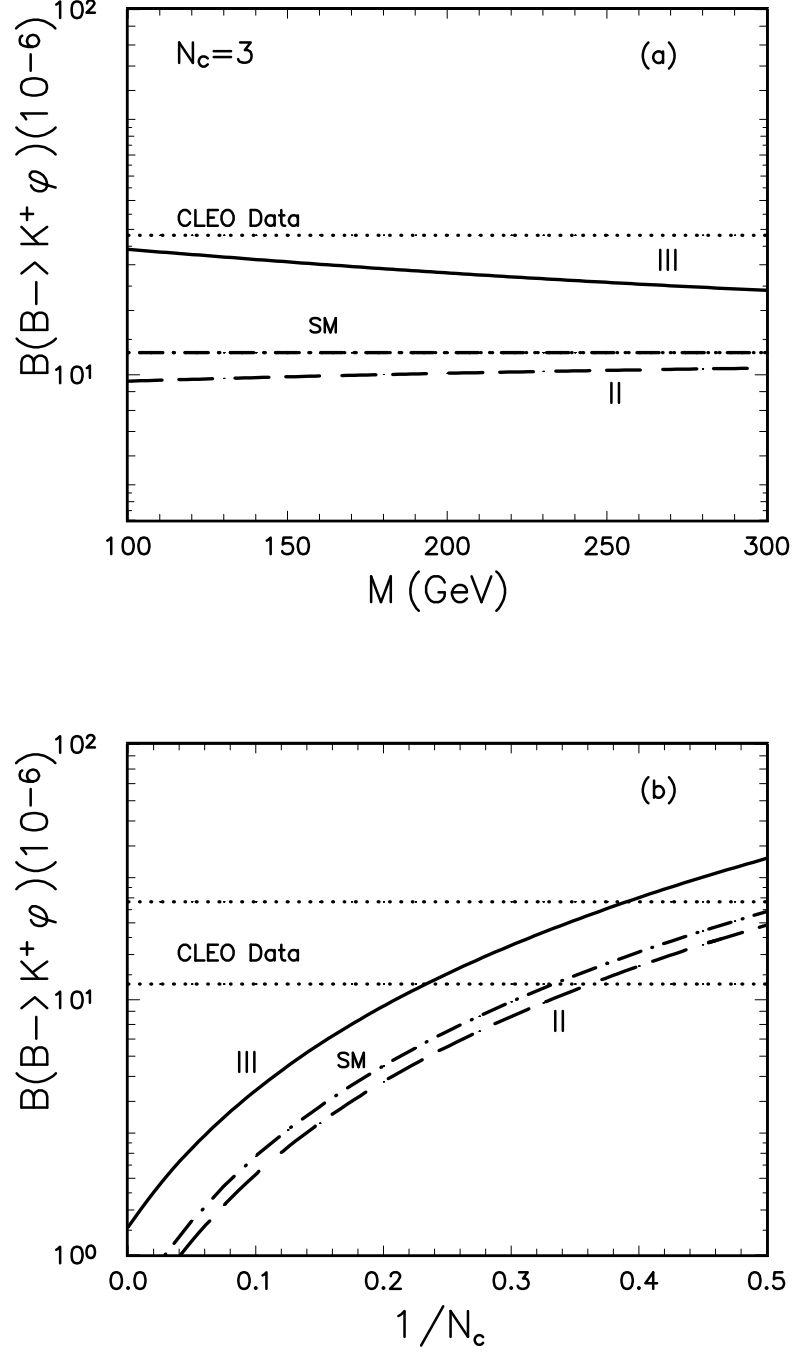


FIG. 14. Same as Fig.11, but for the decay $B \rightarrow K^+ \phi$. The dots band corresponds to the Belle data with 1σ error: $\mathcal{B}(B^+ \rightarrow K^+ \phi) = (17.2^{+6.9}_{-5.7}) \times 10^{-6}$.

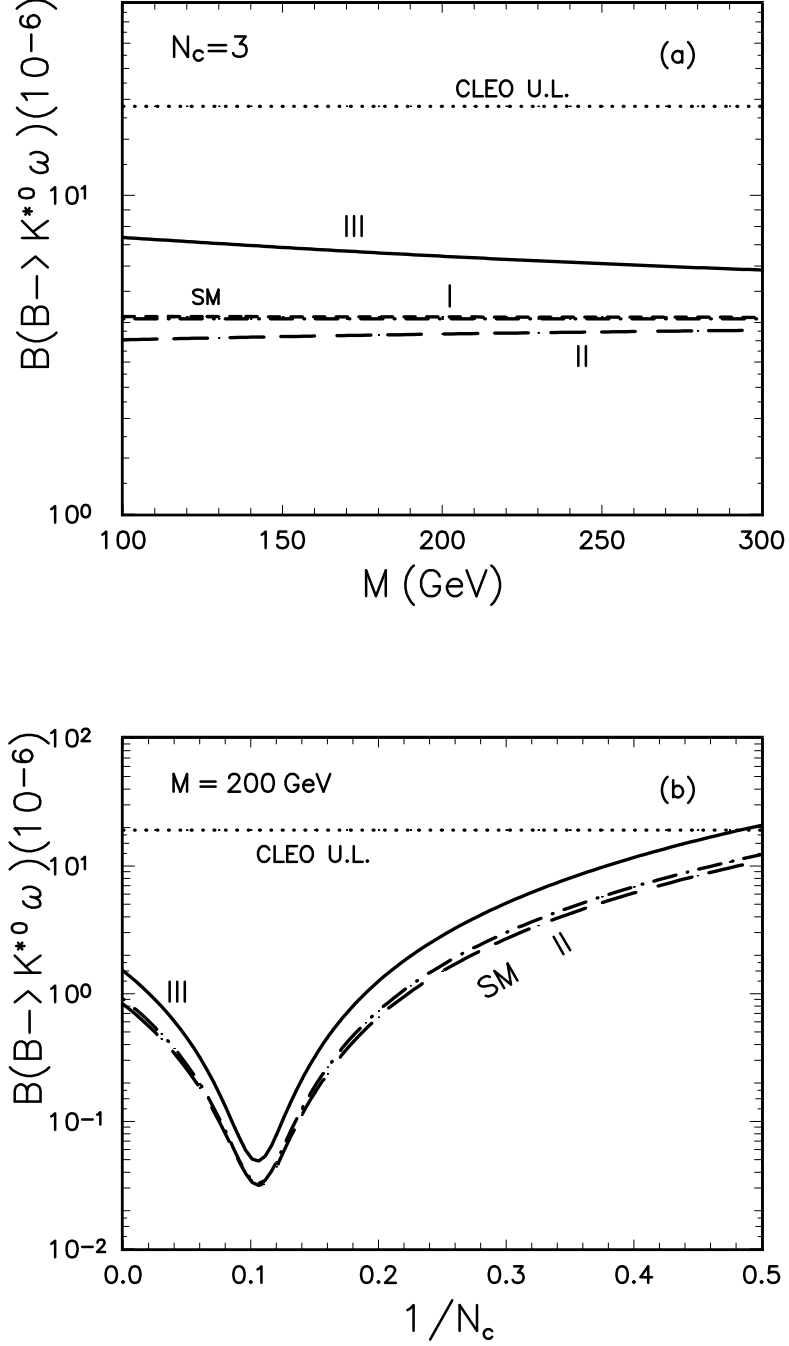


FIG. 15. $\mathcal{B}(B \rightarrow K^{*0} \omega)$ versus M_{H^+} and N^{eff} in the SM and 2HDM's. For (a) and (b), we set $N^{eff} = 3$ and $M_{H^+} = 200$ GeV, respectively. The upper dots line shows the CLEO upper limit: $\mathcal{B}(B \rightarrow K^{*0} \omega) \leq 19 \times 10^{-6}$. The dot-dashed, long-dashed and solid curve corresponds to the theoretical prediction in the SM and models II and III, respectively. The theoretical uncertainties are not shown here.

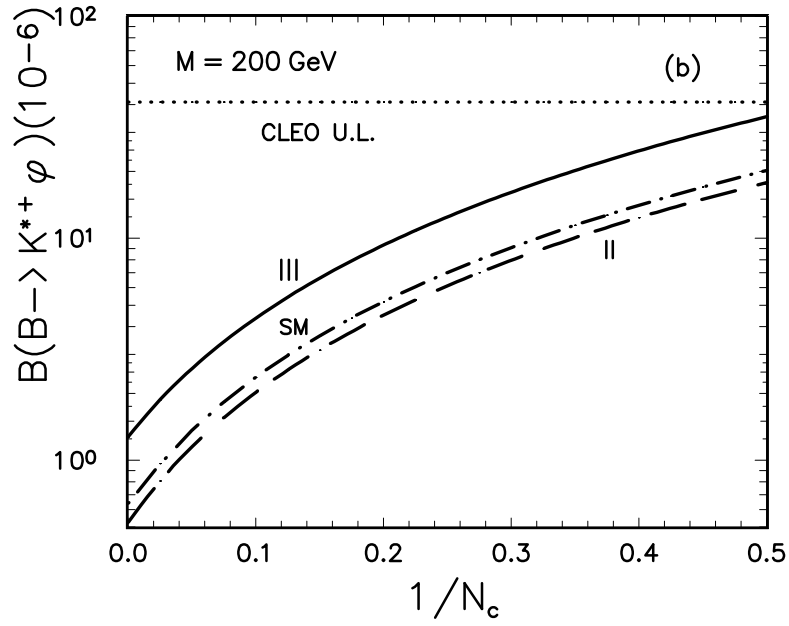
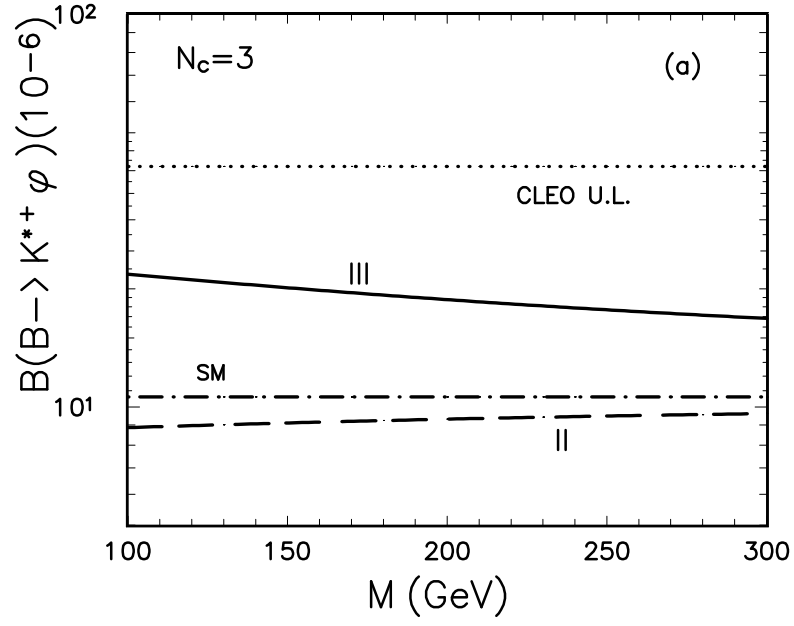


FIG. 16. Same as Fig.15, but for the decay $B \rightarrow K^{*+} \phi$. The upper dots line shows the CLEO upper limit: $\mathcal{B}(B \rightarrow K^{*+} \phi) \leq 41 \times 10^{-6}$.

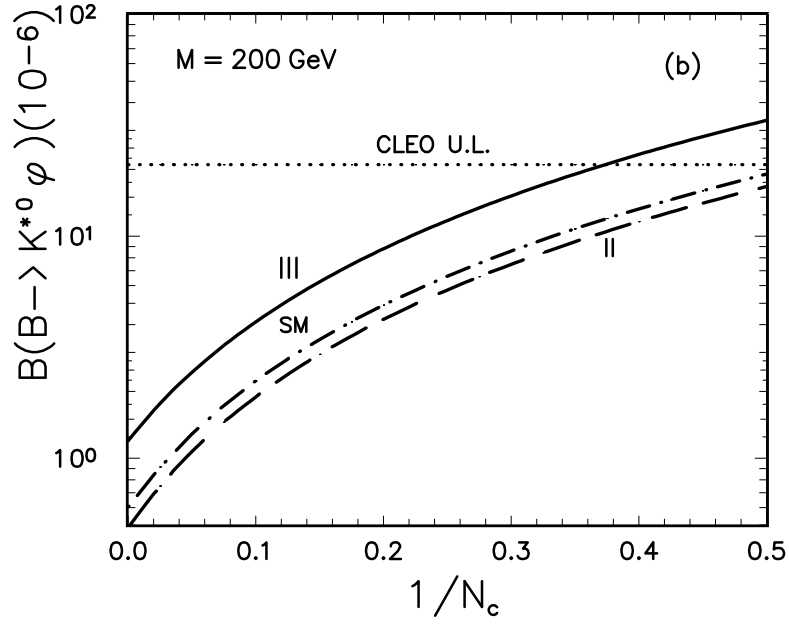
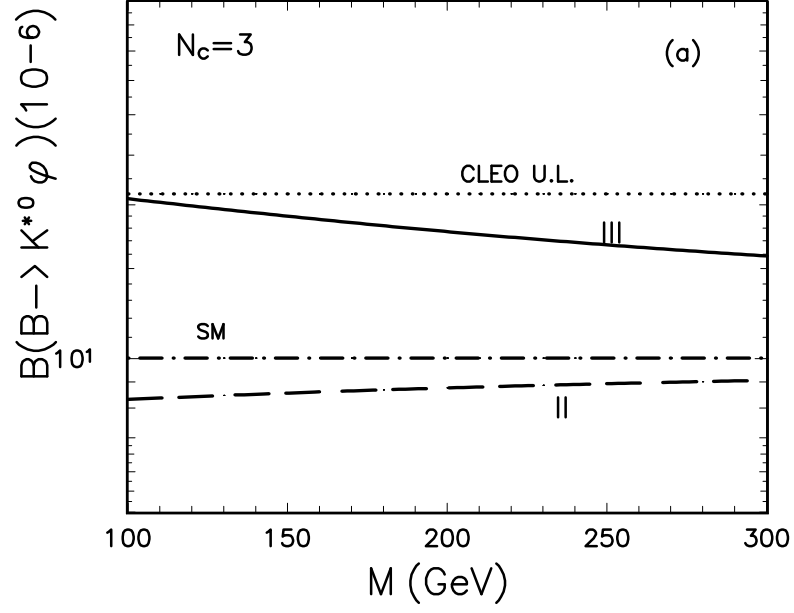


FIG. 17. Same as Fig.15, but for the decay $B \rightarrow K^{*0} \phi$. The upper dots line shows the CLEO upper limit: $\mathcal{B}(B \rightarrow K^{*0} \phi) \leq 21 \times 10^{-6}$.

